JGR Oceans

RESEARCH ARTICLE
10.1029/2022JC018524

Key Points:

- Currents due to the tides' interaction with topography and stratification drive a modest increase in the Indonesian Throughflow (ITF) transports
- Tidal residual circulation drives large but compensatory transports in the three main ITF exit passages
- Tides regulate the partitioning of the ITF amongst its three main exit passages into the Indian Ocean

Supporting Information:

Supporting Information may be found in the online version of this article.

Correspondence to:

A. Katavouta,
annkat@noc.ac.uk

Citation:

Katavouta, A., Polton, J. A., Harle, J. D., & Holt, J. T. (2022). Effect of tides on the Indonesian Seas circulation and their role on the volume, heat and salt transports of the Indonesian Throughflow. *Journal of Geophysical Research: Oceans*, *127*, e2022JC018524. https://doi.org/10.1029/2022JC018524

Received 7 FEB 2022
Accepted 8 JUL 2022

Effect of Tides on the Indonesian Seas Circulation and Their Role on the Volume, Heat and Salt Transports of the Indonesian Throughflow

Anna Katavouta[1,2], Jeff A. Polton[1], James D. Harle[3], and Jason T. Holt[1]

[1]National Oceanography Centre, Liverpool, UK, [2]Department of Earth, Ocean and Ecological Sciences, University of Liverpool, Liverpool, UK, [3]National Oceanography Centre, Southampton, UK

Abstract The effect of tides on the Indonesian Throughflow (ITF) is explored in a regional ocean model of South East Asia. Our model simulations, with and without tidal forcing, reveal that tides drive only a modest increase in the ITF volume, heat and salt transports toward the Indian Ocean. However, tides drive large regional changes in these transports through Lombok Strait, Ombai Strait and the Timor Sea, and regulate the partitioning of the ITF amongst them. The effect of tidal mixing on the salinity and temperature profiles within the Indonesian Seas drives a small decrease in the heat and salt transports toward the Indian Ocean in all three exit passages. In contrast, the tidal residual circulation due to the interaction between the tides and the topography and stratification (including the effects of tidal mixing on the circulation) leads to a large decrease in the transports toward the Indian Ocean through the Lombok and Ombai straits, but a large increase through the Timor Sea. Hence, the small net contribution from tides to the ITF's volume, heat and salt transports is due to a compensation between large, but opposing tidal residual transports at the combined Lombok and Ombai straits and in the Timor Sea. Our results indicate that explicit representation of tides, often missing in Earth system models, is necessary to accurately capture the ITF's pathway and so the tracer transport from the Pacific into the Indian Ocean.

Plain Language Summary As part of the general ocean circulation, water from the Pacific Ocean is transported into the Indian Ocean through the Indonesian Seas. This water enters the Indian Ocean through three exit passages: Lombok Strait, Ombai Strait and the Timor Sea. Here, a model that simulates the ocean conditions and circulation in South East Asia is used to explore the role of tides on this transport of water from the Pacific to the Indian Ocean. We found that although tides have a small influence on the total amount of water transferred from the Indonesian Seas into the Indian Ocean, they drive large changes in the relative amount of water that exits through either the Lombok Strait, Ombai Strait or the Timor Sea. Specifically, the interaction between the tides, the topography and the water's vertical density structure within the Indonesian Seas causes tidally-induced ocean currents that force more water to exit through the Timor Sea, at the expense of less water exiting through the Lombok and Ombai straits. We conclude that the tides regulate the pathway of water exiting into the Indian Ocean through the Indonesian Seas and so may affect the transport of physical, biogeochemical and pollution-related materials in this region.

1. Introduction

The Indonesian Seas are a main pathway of water transport from the Pacific to the Indian Ocean, known as the Indonesian Throughflow (ITF and Figure 1). This water transport is driven by a sea surface gradient between the Pacific and Indian Oceans (Wyrtki, 1987), which is controlled and modulated on seasonal, interannual and decadal timescales by the trade winds, the monsoon winds and the generation and propagation of equatorial waves (Sprintall et al., 2019). The ITF is important for the global ocean circulation and climate, as it is the only low latitude connection between two ocean basins and regulates the heat and freshwater transport associated with the upper meridional overturning branch (Hirst & Godfrey, 1993; Talley, 2008). The ITF primarily consists of North Pacific thermocline water carried into the Indonesian Seas through the Makassar Strait (Gordon et al., 2008, 2010, 2019), with a limited contribution from the South China Sea into the western side of the Java Sea (Fang et al., 2010) (Figure 1). The rest of the ITF enters through the eastern passages of the Molucca Sea and the Halmahera Sea carrying more saline South Pacific water in the thermocline and deeper layers (Gordon

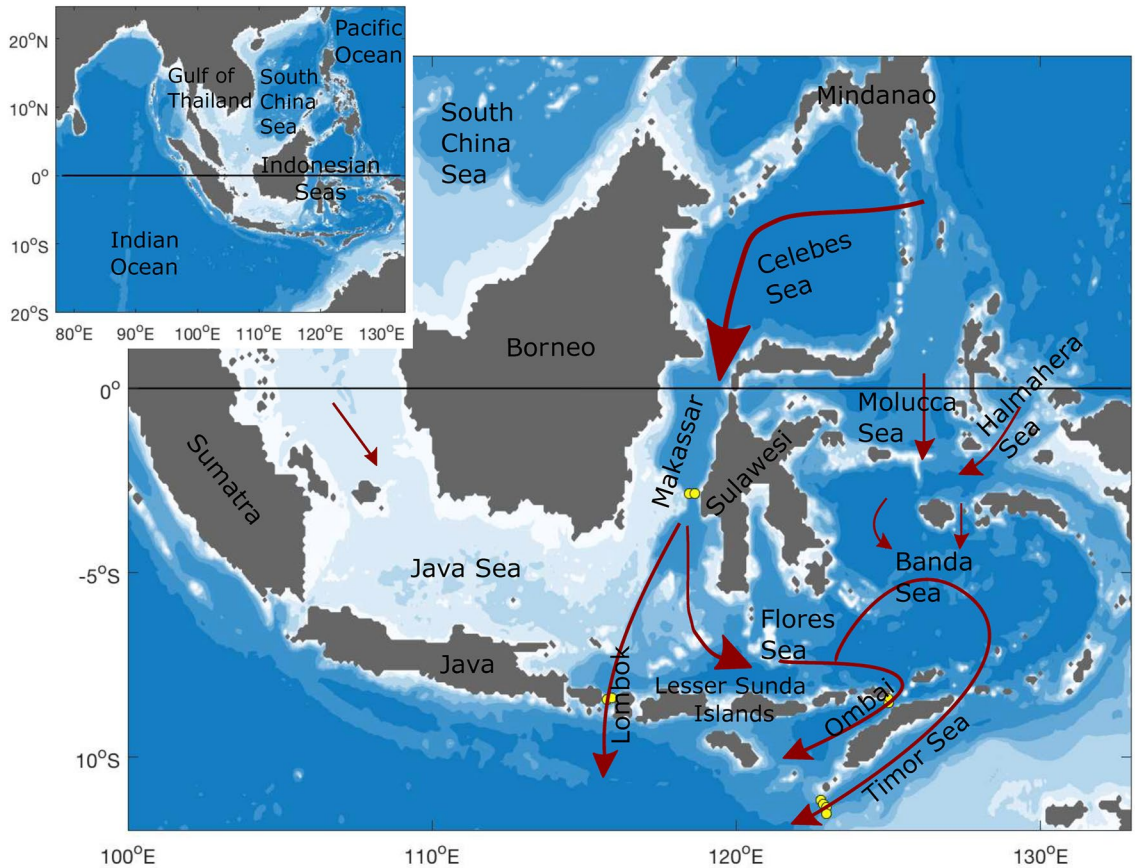

Figure 1. South East Asia model domain (inset-panel), along with a zoom-in on the Indonesian Seas and a schematic of the pathway of the Indonesian Throughflow (dark red arrows). The locations of the observations from the International Nusantara Stratification and Transport program at Makassar Strait, Lombok Strait, Ombai Strait and the Timor Sea are noted with yellow circles.

& Fine, 1996). The majority of the ITF exits into the Indian Ocean through the Lombok Strait, Ombai Strait and the Timor Sea, with a total transport of about 15 Sv (Sprintall et al., 2014).

Enhanced vertical mixing within the Indonesian Seas transforms the Pacific water carried by the ITF into a relatively cool and fresh water mass that can be traced across the Indian Ocean's upper thermocline (Gordon et al., 1997) and intermediate depths (Talley & Sprintall, 2005). The enhanced mixing within the Indonesian Seas is driven by the generation and dissipation of baroclinic tides, as suggested by observations (Ffield & Gordon, 1996; Ray & Susanto, 2016; Robertson, 2010) and modeling studies (Kida & Wijffels, 2012; Koch-Larrouy et al., 2007, 2008; Nagai & Hibiya, 2015; Nugroho et al., 2018; Robertson, 2011; Robertson & Ffield, 2008; Schiller, 2004). This tidally-induced mixing is often parameterized in models, although explicitly including tides in models improves the representation of the water masses and circulation within the Indonesian Seas (Kartadikaria et al., 2011; Schiller, 2004; Tranchant et al., 2016).

The tidal mixing indirectly affects the circulation and ITF transport through changes in the vertical water column's density modifying the sea surface height gradient between the Pacific and Indian Ocean (Sasaki et al., 2018). However, barotropic tides also directly affect the circulation and transport through their interaction with topography that generates persistent residual currents (Huthnance, 1973; Loder, 1980; Polton, 2015). The effect of these barotropic residual currents to the ITF transport is less understood relative to that of the tidally induced mixing, and is ignored in models that include the effect of tides through a mixing parameterization. Limited studies based on coarse resolution models suggest that this barotropic tidal residual current is large within the Indonesian Seas relative to the rest of the global ocean (Bessières et al., 2008) and leads to a relatively large transport along the eastern route of the ITF (Hatayama et al., 1996). Although in coarse resolution models the tides appear to lead to only a modest increase, of 0.7 Sv, in the ITF (Schiller, 2004).

This apparent modest effect of tides on the ITF transport raises two hypotheses: (a) the tides drive significant, but canceling transports through the three main exit passages; and (b) the tides influence the relative contribution of the three exit passages to the ITF. Hence, whilst the tides do not significantly affect the overall magnitude of the ITF, they do control its partitioning between the Lombok Strait, Ombai Strait and the Timor Sea. These hypotheses will have significant implications for the transport of physical (e.g., salinity and temperature), biogeochemical (e.g., carbon, nutrients and oxygen) and pollution-related (e.g., plastics) tracers from the Indonesian Seas into the Indian Ocean. Furthermore, the contribution from the barotropic tidal residual currents to the above tidal effects dictates whether models that do not explicitly include tides, but rather parameterize them in terms of mixing, can realistically capture the ITF.

The above hypotheses motivate us to explore the effect of tides on the volume, heat and salt transports associated with the ITF in the Lombok, Ombai and Timor exit passages using a regional ocean model of South East Asia. Our main aim is to provide insight into the tidally-induced changes in the distribution of the ITF through its three main exit passages, and whether this control is exerted primarily through tidal contributions to mixing or via a modification to the residual currents. In Section 2, our model configuration and experiments are described. In Section 3, we compare the model results with observations in terms of water masses, mean currents and ITF transport. In Section 4, the effect of tides on the volume, heat and salt transports associated with the ITF are investigated in terms of the relative contribution from tidal residual currents and tidal-induced mixing, with focus on tidally-induced changes at the Makassar, Lombok and Ombai straits and in the Timor Sea. Section 5 summarizes our conclusions and discusses the wider context and implications of our study.

2. Model Description and Experiments

2.1. Model Description

The South East Asia model (SEAsia, Figure 1) is a regional configuration of the Nucleus for European Modeling of the Ocean (NEMO, Madec, 2016) version 3.6 with a horizontal resolution of 1/12th degree (~9 km). This resolution is too coarse to accurately represent narrow straits within the Indonesian Seas, and hence the Lombok Strait is somewhat wider in the model, with a width at the ocean surface between 36 km (4 grid points) and 54 km (6 grid points). A resolution of 9 km is not fine enough to resolve the internal tide wavelength in very shallow regions (Holloway, 2001; Robertson & Ffield, 2005), as for example, for M_2 the wavelength is about 14 km in water 100 m deep. Hence, in SEAsia the baroclinic tide will dissipate locally rather than propagating accurately in very shallow regions. The chosen 9 km resolution is a compromise for conducting long term sensitivity experiments in our relative large domain, while partially resolving the internal tide propagation.

In the vertical, the model has 75 levels that follow a hybridization between z* (geopotential-following, with a non-linear free surface) and σ (terrain-following) coordinate systems. In the open ocean (deeper than 430 m) the model employs z* coordinates with partial steps, whereas in the regions shallower than 430 m the vertical coordinates switch to σ. The stretching function of the σ coordinates makes use of the underlying analytical function used to describe distribution in the z* coordinates. Of the 75 levels, the upper 39 become σ, transitioning to a pure σ (i.e., all layers have equal thickness) in waters shallower than 39 m. A minimum and maximum bottom depth of 10 and 6,000 m is maintained and a slope parameter (rmax; a measure of bathymetric gradient) of 0.05 is enforced. In regions where the slope parameter is exceeded, a vanishing-quasi-sigma method is employed to constrain bathymetric steepness and hence horizontal pressure gradient error (see Wise et al., 2022, for further details). The model bathymetry is a merge of ETOPO2 (National Geophysical Data Center, 2006) and GEBCO1 (IOC, IHO & BODC, 2003) and was chosen to match that of the ORCA12 simulations within the DRAKKAR consortium (DRAKKAR Group, 2007) that are used to force our regional model. A minimum depth of 10 m is specified for the model's bathymetry to avoid problems with the tidal range as there is no implementation of wetting/drying in the model.

The model implements a non-linear free surface using the variable volume layer scheme (Levier et al., 2007) and time-splitting with a baroclinic time-step of 360 s and a barotropic time-step chosen as to satisfy a maximum Courant number of 0.5. A Laplacian lateral eddy diffusion scheme with a coefficient of 125 $m^2\ s^{-1}$ is used for tracers and a bi-Laplacian lateral eddy viscosity scheme with a coefficient of $1.25 \times 10^{10}\ m^4\ s^{-1}$ is used for momentum. The Generic Length Scale (GLS) turbulent closure scheme (Umlauf & Burchard, 2003) with a k-ϵ predefined turbulence model and the Canuto et al. (2001) stability function is used for the parameterization of

Table 1
South East Asia Model Experiments

Experiment	Time	Atmospheric forcing	Ocean forcing	River forcing	Tidal forcing
SEAsia-tide	1981–2012	DFS5.2	ORCA0083-N006	Climatology	FES2014
SEAsia-NOtide	1981–2012	DFS5.2	ORCA0083-N006	Climatology	NO
SEAsia-BTtide	3 years	NO	NO, uniform T & S	NO	FES2014

vertical diffusion of tracers and momentum. A non-linear (quadratic) bottom friction is used with a bottom drag coefficient of 2.5×10^{-3}. At the model's open lateral boundaries, a flow relaxation scheme is applied to relax the model's temperature and salinity to external values along a 10 grid points zone. The Flather radiation condition (Flather, 1994) is used to introduce the barotropic velocities and the sea surface height, while the baroclinic velocities are specified along the open lateral boundaries.

2.2. Model Experiments

Three simulations where conducted using the SEAsia model to investigate the effect of tides (Table 1): (a) a simulation with tides (SEAsia-tide), (b) a simulation without tides (SEAsia-NOtide), and (c) a simulation forced only by the barotropic tide (SEAsia-BTtide).

2.2.1. SEAsia-tide

The SEAsia-tide simulation is forced by external ocean conditions at the open lateral boundaries, atmospheric conditions at the surface, river run-off and tides. The temperature, salinity, sea surface height and currents forced at the open lateral boundaries are based on 5-day averages from the global 1/12th degree ORCA0083-N06 simulation conducted by the National Oceanography Centre, UK (Moat et al., 2016). Precipitation, winds, air humidity, air temperature, and downward shortwave and longwave radiation from the DRAKKAR Forcing sets-DFS5.2 (Dussin et al., 2016) are used to force the heat, freshwater and momentum fluxes from the atmosphere to the ocean surface. Specifically, these air-sea fluxes are estimated using NEMO's bulk flux parameterization (NCAR, Large & Yeager, 2009). The DFS5.2 forcing set is based on the ERA-interim global atmospheric reanalysis, with additional corrections described in Dussin et al. (2016). River forcing is applied using a monthly climatology of river run-off based on Dai and Trenberth (2002). The model is also forced by 34 tidal constituents taken from the FES2014 tide model (Lyard et al., 2021, all 34 constituents available by FES2014). Tidal forcing is applied as a tidal potential and as a sea surface height and barotropic currents condition along the model's open lateral boundaries. This simulation is for years 1981–2012 starting from a spin up state based on 21 years (1960–1980).

2.2.2. SEAsia-NOtide

The SEAsia-NOtide simulation is identical to the SEAsia-tide simulation, excluding tides. The eddy parameterization is kept the same as in the SEAsia with tides simulation and we do not apply any additional parameterization or bottom drag for tidal mixing. SEAsia-NOtide is run for years 1981–2012 starting from a spin up state based on 21 years (1960–1980).

2.2.3. SEAsia-BTtide

The SEAsia-BTtide simulation is a 3 year simulation forced only by the barotropic tide. In this simulation 34 tidal constituents taken from FES2014 are applied as a tidal potential and along the model's open lateral boundaries, as in the SEAsia-tide run, but this simulation is initialized with a spatially uniform temperature and salinity and there is no oceanic, atmospheric or river forcing except where the effect is represented by the FES2014 harmonics. This simulation is a barotropic simulation but not a depth-averaged simulation as it has 75 vertical levels and includes the effect of bottom friction and vertical diffusion of momentum.

3. Representation of the Indonesian Seas and Indonesian Throughflow in the SEAsia Model

The current set-up of the SEAsia model at a resolution of 1/12° is designed for long-term sensitivity experiments that enable mechanistic understanding rather than to provide the most realistic hindcasts. Nevertheless, the model should be able to capture the hydrography and circulation in the Indonesian Seas, at least in terms of broad spatial patterns and low frequency variability, and provide an insight into the effects of tides on the ITF. In this section, the SEAsia model is validated against observations, with the focus on seasonal variability and climatological averages. The influence of tides on the model's representation of the ocean conditions within the Indonesian Seas is also briefly discussed in this section; however, a more thorough discussion of the effect of tides is reserved for Section 4.

3.1. Tides

The SEAsia model simulates the amplitude and phase of the 4 main tidal constituents in agreement with FES2014 (Figure 2); this is the case for the rest of the 34 tidal constituents (not shown). The imprint of the baroclinic tides, not present in FES2014, is evident in the 4 tidal constituents, as shown by the regional striation patterns in their amplitude (Figure 2). In the SEAsia model, the tide is predominatly semi-diurnal in the Indonesian Seas and diurnal to the North of the Java Sea up to the South China Sea, which is consistent with FES2014, previous modeling studies (Kartadikaria et al., 2011) and data assimilation products (Ray et al., 2005).

On the south side of the Indonesian Seas, the semi-diurnal tide (M_2 and S_2) enters from the Indian Ocean and propagates from the Banda Sea toward the Flores Sea (Figures 2a and 2b). On the north side of the Indonesian Seas, the M_2 and S_2 tides enter through the Pacific Ocean and propagate South through the Makassar Strait. SEAsia-tide simulates well the location of the amphidromic points in the semi-diurnal tides within the Gulf of Thailand, in the Java Sea and in the Timor Sea (Figures 2a and 2b). However, in the SEAsia-tide the semi-diurnal tide amphidromic point near the west coast of Sumatra is simulated further offshore between Malaysia and Borneo. The model's M_2 and S_2 amplitudes are large in the Celebes and Banda seas, with M_2 amplitude reaching more than 50 cm, but generally less than 20 cm in the Flores and Java seas where the tide propagating from the Pacific Ocean meets the tide propagating from the Indian Ocean. This is overall consistent with FES2014 (Figures 2a and 2b), however the model overestimates the M_2 amplitude by about 20 cm in the Celebes Sea.

The diurnal tide (K_1 and O_1, Figures 2c and 2d) enters through the Pacific Ocean into the Indonesian Seas and propagates southwards toward the Banda and Flores seas, where it meets the tide coming from the Indian Ocean. SEAsia-tide has a diurnal tide amphidromic point within the Gulf of Thailand at the same location with FES2014. The model simulates the decrease in K_1 and O_1 amplitudes westwards of the Java Sea and in the Banda Sea, consistent with FES2014. However, the model overestimates the amplitude of the diurnal tide south of the Gulf of Thailand and along the east side of Sumatra (Figures 2c and 2d).

Overall, the model's tidal amplitude and phase are in good agreement with those obtained from the Global Extreme Sea Level Analysis (GESLA, Piccioni et al., 2019) sea-level tide gauges record (Figures S1 and S2 in Supporting Information S1), with a relatively small root mean square error (RMS) (Table 2). However, these comparisons confirmed that the model overestimates the K_1 and O_1 amplitudes, particularly in regions with large diurnal tide like in the Gulf of Thailand, north of Borneo and along the coast of Malaysia.

To evaluate the SEAsia tidal velocities, the tidal ellipses' major axes from the SEAsia-tide are compared with those based on observations from the International Nusantara Stratification and Transport program (INSTANT, Gordon et al., 2008; Sprintall et al., 2009). The estimates of the observed major axes were determined for both the "raw" data and data on constant pressure surfaces from the INSTANT program, following Robertson (2010). Note that the estimates based on the INSTANT observations have some limitations due to strong currents "pulling" the instruments much deeper than their nominal depths (Robertson, 2010). SEAsia-tide captures well the observed vertical structure of the diurnal and semi-diurnal major axes at Makassar, Lombok and Ombai straits, particularly in terms of the constant pressure surfaces data (Figures S3, S4, and S5 in Supporting Information S1). In the Timor Sea the model overestimates the major axes magnitude, but the baroclinic tide is weak in both the observations and SEAsia-tide (Figures S6 and S7 in Supporting Information S1). The overall reasonable agreement between the observed and SEAsia tidal currents in terms of vertical structure provides confidence in the

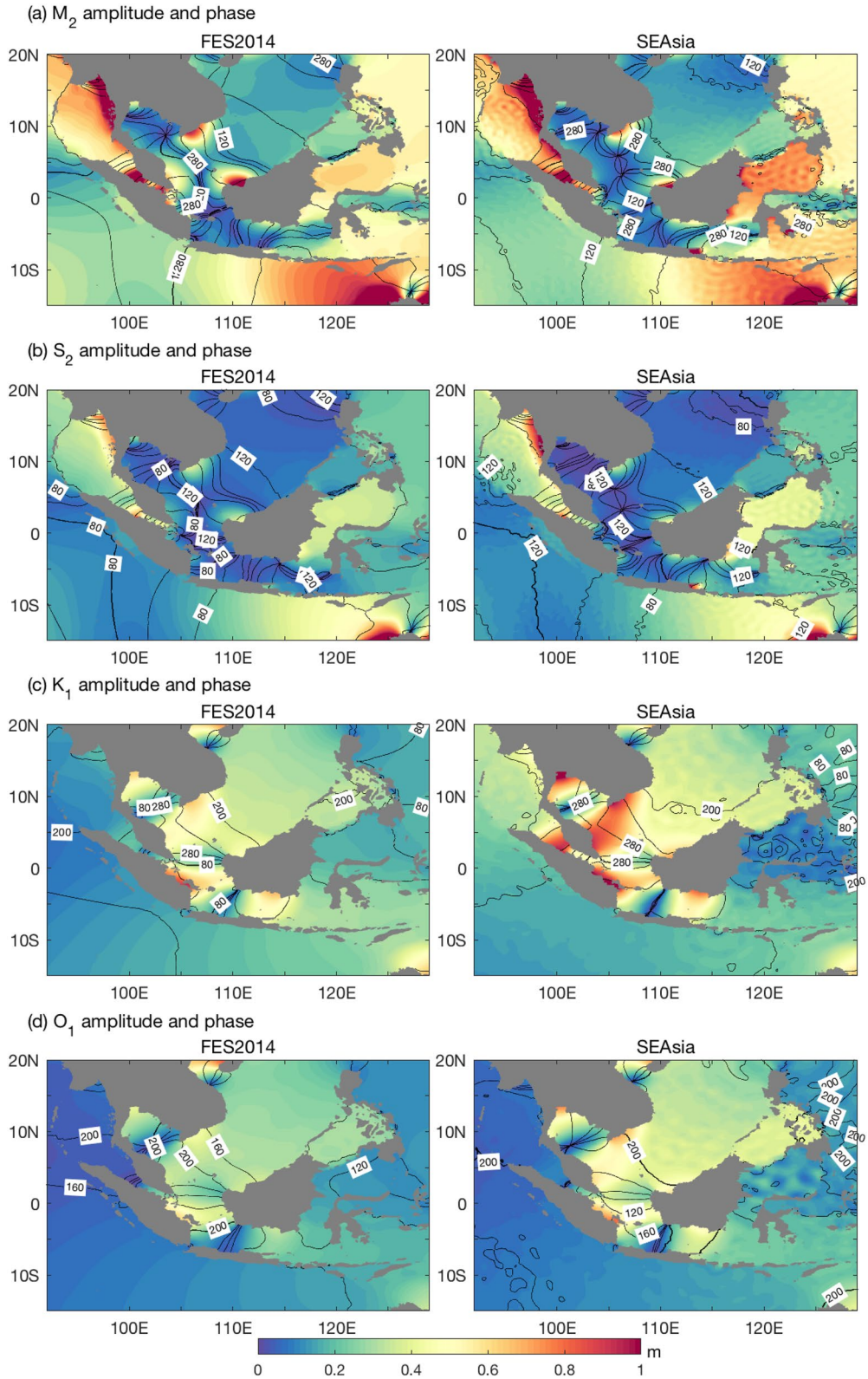

Figure 2. Amplitude (m) and phase (degrees) for four tidal constituents from FES2014 and South East Asia model-tide: (a) M_2, (b) S_2, (c) K_1, and (d) O_1.

Table 2
The Root Mean Square Difference Between the South East Asia Model-tide and the Observed M_2, S_2, K_1, and O_1 Amplitude and Phase

Constituent	Amplitude (cm)	Phase (degrees)
M_2	25.7	34
S_2	13.6	40
K_1	15.0	32
O_1	6.5	26

Note. The observed tidal elevations are based on the Global Extreme Sea Level Analysis (GESLA) sea-level tide gauges record.

representation of the baroclinic tides in the model; although we highlight that a model resolution of order of 1 km is necessary to simulate accurately the baroclinic tide propagation in shallow regions.

3.2. Water Masses

To validate the model water masses within the Indonesian Seas we compare the model simulations with temperature and salinity climatology from the World Ocean Atlas (WOA2018) (Boyer, García, et al., 2018, 1981–2010 period) and ocean profile data from the World Ocean Database (WOD2018) (Boyer, Baranova, et al., 2018). Specifically, we examine (a) the salinity along the western and the eastern paths of the ITF (Figures 3a and 3b), (b) the salinity at the 1025.5 kg m^{-3} isopycnal (Figure 3c), and (c) temperature-salinity diagrams for different regions within the Indonesian Seas (Figure 4).

Along the western path of the ITF, North Pacific Subtopical Water, characterized by a salinity of about 34.8–35.0 PSU, enters within the upper thermocline (50–200 m) into the Celebes Sea, while fresher (34.2–34.5 PSU) North Pacific Intermediate Water enters within the lower thermocline (Figure 3a). In the Celebes Sea, SEAsia-tide captures the characteristic signature of North Pacific water, that is, high salinity water overlying fresher water, in good agreement with the observations (Figures 3a and 4a). SEAsia-tide has a somewhat higher salinity within the mixed-layer than the observations in the Celebes Sea (Figures 3a and 4a). As the water moves south into the Makassar and Lombok straits, mixing erodes its stratification in both the observations and SEAsia-tide (Figure 3a). At the Makassar and Lombok straits, SEAsia-tide robustly captures the observed salinity profile and the low salinity at the surface (≤33.8 PSU) associated with freshwater outflow from the Java Sea (Koch-Larrouy et al., 2008); however, in SEAsia-tide the relative cool water (≤10°C) found below 300 m is slightly more saline than in the observations (Figures 3a and 4b).

Along the eastern path of the ITF, South Pacific water enters mainly through the Halmahera Sea. This water consists of high salinity (≥35 PSU) South Pacific Subtropical water within the upper thermocline and fresher South Pacific Intermediate water within the lower thermocline (Figure 3b). The salinity gradient of these water masses is strongly eroded before reaching the Banda Sea (Figure 3b) due to intense tidal mixing (Koch-Larrouy et al., 2007; Nagai et al., 2021). Within the Banda Sea, this water from the South Pacific is further mixed with water penetrating from the western path of the ITF; which results in a water mass that is relatively well-mixed but more saline than the water in the western path of the ITF, in both the observations and SEAsia-tide (Figure 3b). However, SEAsia-tide overestimates the salinity near the surface relative to the observations in the Banda Sea (Figures 3b and 4c).

At the Ombai Strait and in the Timor Sea, SEAsia-tide is in good agreement with the observations (Figure 4d). SEAsia-tide accurately captures the characteristic almost isohaline water mass below 20°C. At greater depth, a salinity maximum in water with temperature <10°C is evident in the observations and the SEAsia-tide (Figure 4d), which is associated with influence from the South Pacific water. However, this salinity maximum is more pronounced in SEAsia-tide than in the observations. Near the surface SEAsia-tide overestimates the salinity which is partly associated with regional variability within the Timor Sea. In the Indian Ocean south of the Lombok Strait, SEAsia-tide captures the observed water mass profile and the characteristic signature of the ITF with salinity of about 34.5–34.7 PSU in the upper thermocline and intermediate depths (Figure 4e). SEAsia-tide captures (consistent with the climatology) the ITF spreading westwards into the Indian Ocean within the upper thermocline between 15°S and 12°S, becoming saltier as it mixes with surrounding waters (Figure 3c); but this signature of the ITF within the Indian Ocean is slightly weaker in the model.

Overall, within the Indonesian Seas and in the vicinity of the exit of the ITF into the Indian Ocean SEAsia-tide overestimates the salinity near the surface by about 0.4 PSU (Figure 4f) and the salinity error reaches maximum at the surface (Figure 4g), which is probably associated with local inaccuracies in the air-sea freshwater flux in the model. The SEAsia-tide bias and error in salinity decreases with depth, with an overestimation of less than 0.2 PSU in the upper thermocline below 150 m, and an underestimation of less than 0.02 PSU below 500 m (Figures 4f and 4g). SEAsia-tide is warmer by about 0.4°C at the surface than the observations and overestimates the temperature within the upper thermocline below 100 m (Figure 4f). In contrast, SEAsia-tide is cooler than the

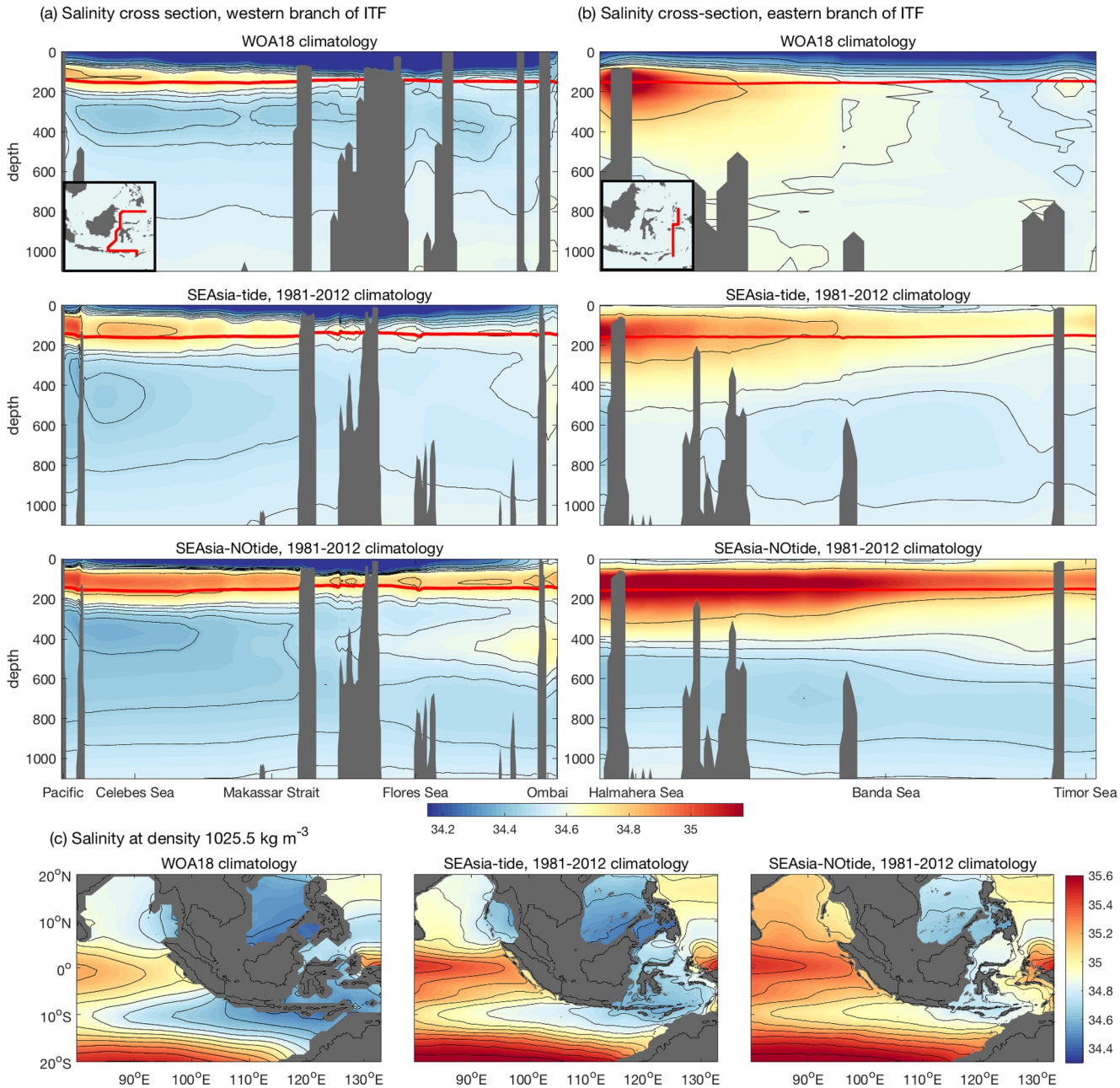

Figure 3. Salinity climatology cross-sections through the Indonesian Seas: (a) western branch of the Indonesian Throughflow (ITF), (b) eastern branch of the ITF, and (c) at the 1025.5 kg m^{-3} isopycnal, from the World Ocean Atlas (1981–2010 period), South East Asia model (SEAsia)-tide and SEAsia-NOtide based on years 1981–2012. The top inset-panels show the location of the sections through the Indonesian Seas. The red line in the salinity cross-section figures denotes the 1025.5 kg m^{-3} isopycnal.

observations between 50 and 100 m and below 750 m (Figure 4f). The SEAsia-tide temperature error is larger within the upper thermocline (Figure 4g).

In the absence of tides, SEAsia-NOtide retains an unrealistic stratification throughout the Indonesian Seas, consistent with previous studies (Kartadikaria et al., 2011; Koch-Larrouy et al., 2007; Nugroho et al., 2018; Tranchant et al., 2016), with an unrealistically high salinity within the upper thermocline and low salinity within the lower thermocline (Figure 3a, 3b and Figure 4a–4e). The freshwater signature of the ITF within the Indian Ocean is less pronounced in the absence of tides, with salinities reaching more than 34.8 PSU in the vicinity of the

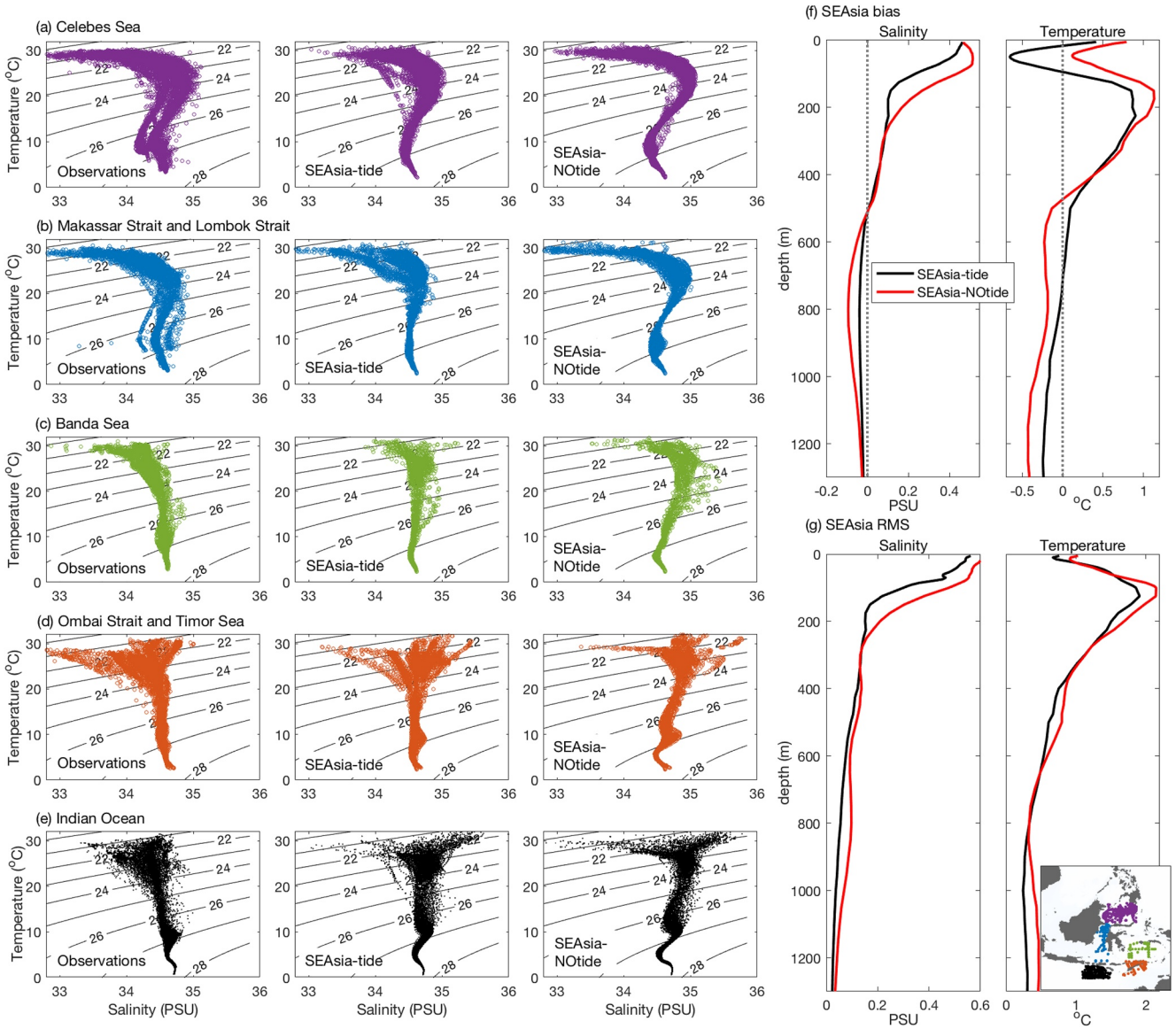

Figure 4. Temperature-Salinity diagrams from the observations, South East Asia model (SEAsia)-tide and SEAsia-NOtide for the: (a) Celebes Sea, (b) Makassar and Lombok straits, (c) Banda Sea, (d) Ombai Strait and Timor Sea, and (e) Indian Ocean, along with the (f) model bias (positive for model overestimation) and (g) model root mean square error for temperature and salinity (combined for all locations). The observations are from the World Ocean Database and for different seasons and years (between 1981 and 2012). The bottom right inset-panel shows the location of the observations. The model temperature and salinity are spatially and temporally matched with the observations.

outflow (Figure 3c). Overall, SEAsia-tide is in better agreement with the observations than the SEAsia-NOtide (i.e., SEAsia-tide exhibits a lower bias and RMS, Figures 4f and 4g).

3.3. Circulation

3.3.1. General Circulation

The general circulation in the Indonesian Seas is characterized by the flow from the Pacific Ocean toward the Indian Ocean (i.e., ITF, schematic in Figure 1). SEAsia-tide broadly captures this tendency of flow toward the Indian Ocean all year round (Figure 5a). In the western route of the ITF, SEAsia-tide simulates the western boundary current along Mindanao transferring water into the Celebes Sea that then continues Southwards into the Makassar Strait (Figure 5a). In the western side of the Celebes Sea there is inflow from the South China Sea that

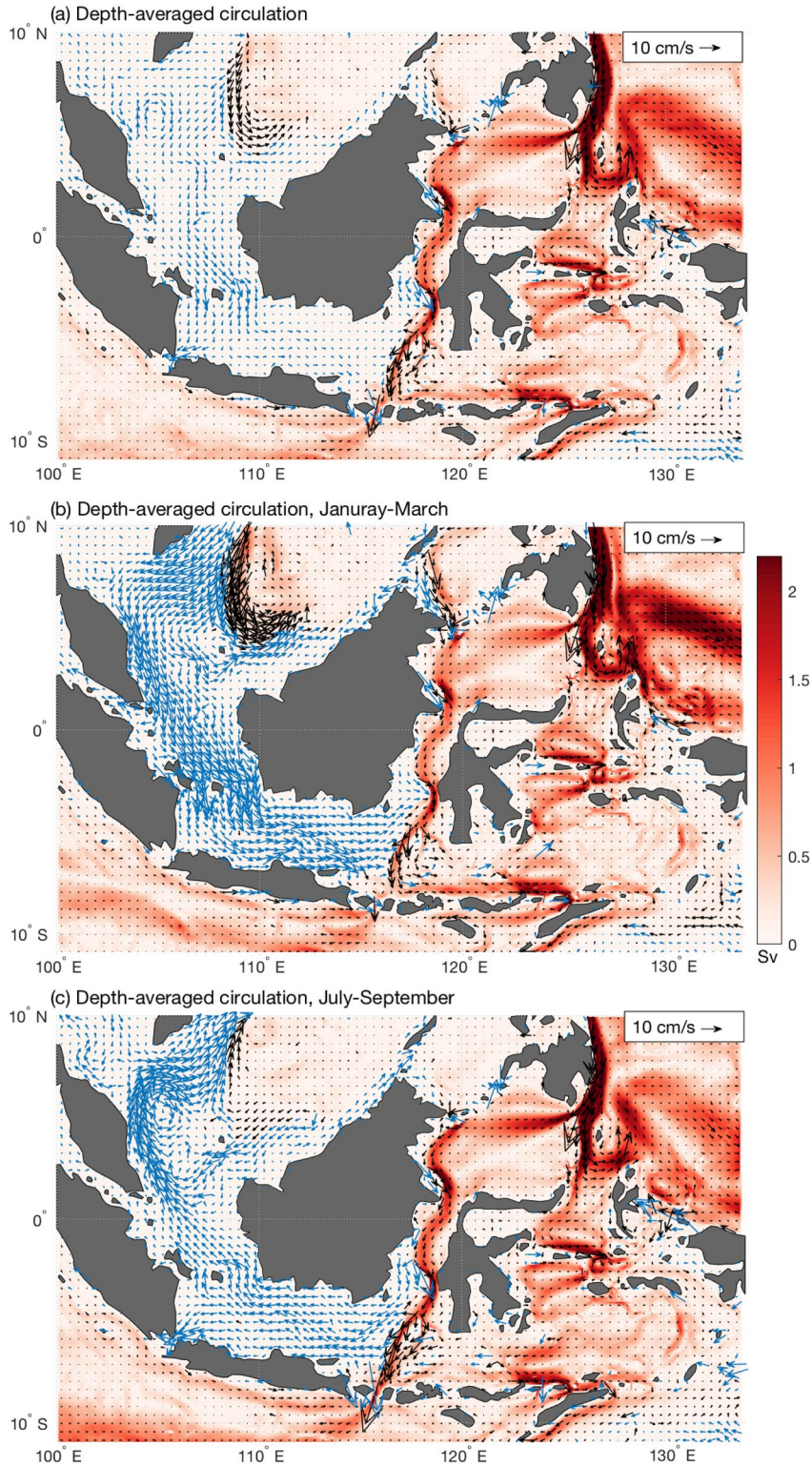

Figure 5. Depth-averaged circulation in the Indonesian Seas for (a) the whole year, (b) winter (January–March) and (c) summer (July–September) in South East Asia model-tide. The circulation estimates are based on years 1981–2012. The blue arrows show circulation in regions with bathymetry less than 100 m and the black arrows show circulation in regions with bathymetry deeper than 100 m. The color-scheme shows the magnitude of the volume transport.

is restricted to the upper thermocline and intensifies during the boreal winter (Figure 5b) due to more Kuroshio water intruding into the South China Sea (Wei et al., 2016). This water flow from the South China Sea acts as a "freshwater plug" reducing the inflow from the Mindanao Current into the Makassar Strait (Gordon et al., 2012; Wei et al., 2016) and consequently, the flow southwards from the Makassar Strait is also reduced during winter (Figure 5b).

A portion of the flow from the Makassar Strait continues southwards exiting into the Indian Ocean through the Lombok Strait while the rest shifts eastwards toward the Flores Sea (Figure 5a). In the shallow Java Sea the circulation is south-eastwards during the boreal winter, but shifts to north-westwards during the boreal summer (Figures 5b and 5c) driven by the seasonal reversal of the monsoon winds. This freshwater outflow from the South China Sea through the Java Sea during winter contributes to the reduction of the southward flow from the Makassar Strait (the "freshwater plug" concept, Gordon et al., 2012) and contributes to a larger portion of this flow turning eastwards rather than exiting directly into the Indian Ocean through the Lombok Strait in the model.

Along the eastern path of the ITF, North Pacific water enters via the Molucca Sea and South Pacific water via the Halmahera Sea where complex topography leads to clockwise and anti-clockwise currents in SEAsia-tide (Figure 5a). The water then flows into the Banda Sea where it meets water coming from the Makassar Strait via the Flores Sea. The water coming from the west enters the Banda Sea mainly within the upper 500 m in the model, consistent with the study of Liang et al. (2019).

3.3.2. Currents at the Makassar, Lombok and Ombai Straits and in the Timor Sea

Observations from the INSTANT program are used to assess the model's currents at the Makassar Strait and the three main exit passages of the ITF. Specifically, we compare the vertical profiles of the along-channel currents from the observations, SEAsia-tide and SEAsia-NOtide (Figure 6).

At the Makassar Strait, SEAsia-tide captures the vertical structure of the southward flow with the along-channel current velocity reaching maximum (0.6 m/s) within the upper thermocline (100–200 m) and decreasing below 200 m (Figures 6a–6c). However, SEAsia-tide simulates a sharper decline in the current speed with depth than observed. A western intensification of the current is evident in both the observations and SEAsia-tide (Figure 6b). At the Lombok Strait, the flow is southwards and mainly confined to the upper 300 m in SEAsia-tide and the observations (Figures 6d–6f). SEAsia-tide also captures the current maximum speed within the upper 100 m at the western side and the reduction in the current speed at the eastern side of the Lombok Strait. At the Ombai Strait, SEAsia-tide captures the strong upper current toward the Indian Ocean at the southern side, and the current reversal toward the Indonesian Seas below 300 m at the northern side (Figures 6g–6i). This flow reversal has been attributed to the South Java current and undercurrent extending eastwards into the Ombai Strait (Sprintall et al., 2010). However, at the northern side of Ombai Strait, SEAsia-tide overestimates the current reversal below 300 m and has a current of opposite sign to that observed near the surface. In the Timor Sea, the flow in the SEAsia-tide is toward the Indian Ocean, with a strong core flow confined within the upper 300 m and a secondary weaker flow at depths between 600 and 1500 m, consistent with the observations (Figures 6j–6l). Near the bottom the current is toward the Indian Ocean in both the observations and the SEAsia-tide, however, the model underestimates this current speed.

At the Lombok and Ombai straits and in the Timor Sea the currents vertical structure in SEAsia-tide is in better agreement with the observations than in the SEAsia-NOtide, with a smaller RMS (Figures 6e, 6f, 6h, 6k, and 6l). The exception is Ombai North where, while the vertical profile is more realistic in the SEAsia-tide, near the surface SEAsia-tide overestimates the current by about 0.5 m s^{-1} (Figure 6i). Notably, in the absence of tides the model has a current reversal extending throughout the Ombai Strait, but confined between 400 and 600 m (Figures 6g and 6i). In contrast in the SEAsia-tides and observations this current reversal is found only at the north side of the Ombai Strait and at depths extending from 300 to 1000 m. At the Makassar Strait, the effect of tides is small (Figures 6a–6c).

3.4. Indonesian Throughflow

Volume, heat and salt transports in the model are estimated based on 5-day averaged currents, temperature and salinity as

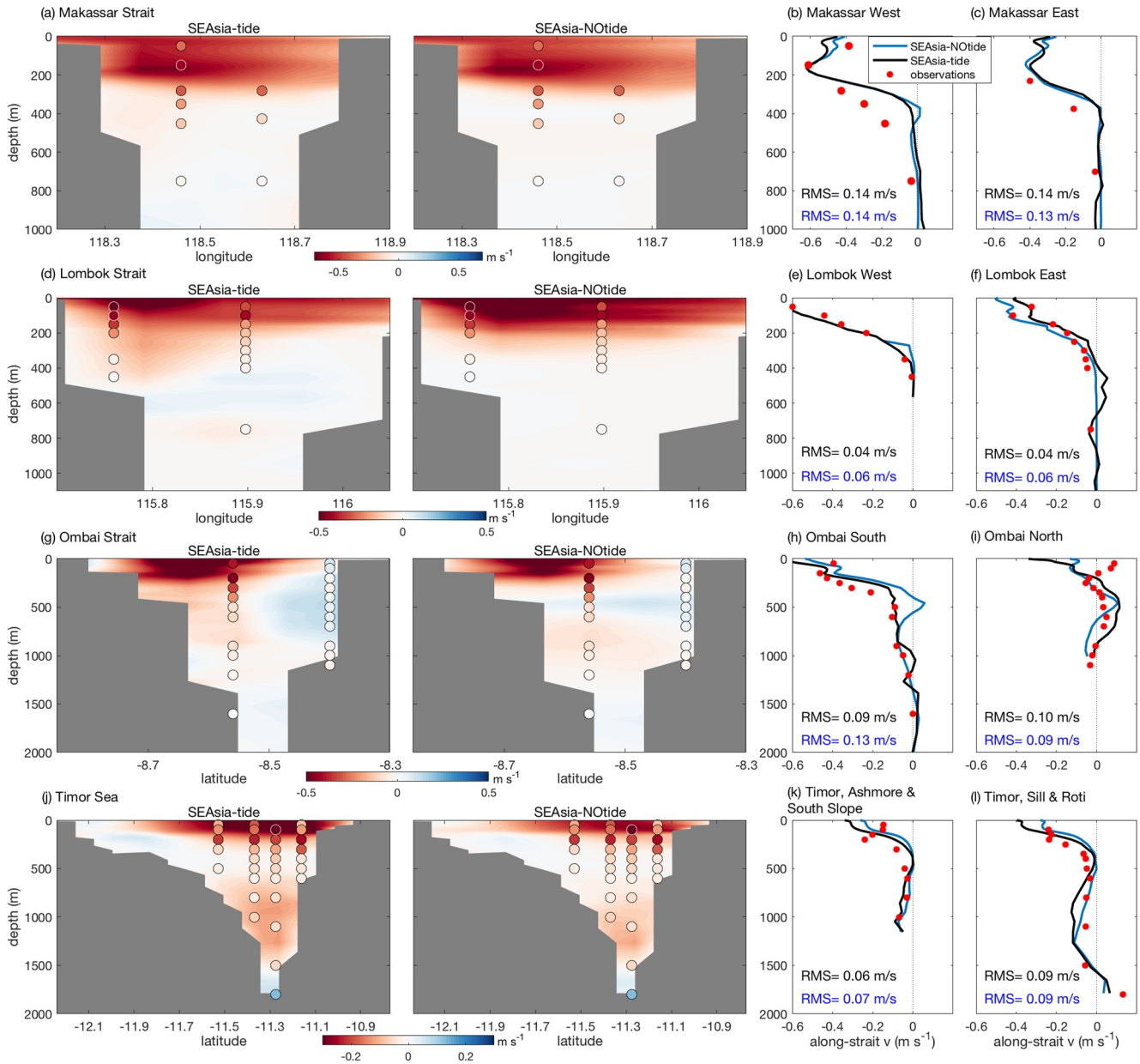

Figure 6. Along-strait current: (a) Makassar Strait, (d) Lombok Strait, (g) Ombai Strait, and (j) the Timor Sea from South East Asia model (SEAsia)-tide and SEAsia-NOtide, along with observations shown by the color circles. Comparison of the vertical along-strait current profiles at the location of the observations: (b) Makassar West, (c) Makassar East, (e) Lombok West, (f) Lombok East, (h) Ombai South, (i) Ombai North, (k) Timor Ashmore and South Slope (the two southern-most locations) and (l) Timor Sill and Roti (the two northern-most locations). The root mean square error for the SEAsia-tide and SEAsia-NOtide is also reported (black and blue, respectively) for each of the locations. The observations are from the International Nusantara Stratification and Transport program for years 2004–2006. The model currents are estimated based on years 2004–2006, for consistency with the observations. Red color denotes flow toward the Indian Ocean.

$$\text{Volume transport} = \int udA, \tag{1}$$

$$\text{Heat transport} = c_p \int \rho\theta udA, \tag{2}$$

$$\text{Salt transport} = \int \rho S udA, \tag{3}$$

where u, ρ, θ and S are the normal velocity to the area dA (m s^{-1}), density (kg m^{-3}), potential temperature (°C) and salinity (PSU), respectively, and $c_p = 4 \times 10^3$ J°C^{-1} kg^{-1} is the specific heat capacity (taken as a constant).

The heat and salt transports estimated from Equations 2 and 3 correspond to an "absolute transport" referenced to 0°C temperature and 0 PSU salinity, which captures the total tracer transport through a section. In terms of heat and freshwater budgets it is often meaningful to consider estimates of heat and salt transport referenced to a "closure" section of return flow. Here, we focus on transport in the "absolute sense" (i.e., referenced to 0°C and 0 PSU) in order to (a) highlight the effect of changes in the circulation due to tides on the total tracer transport from the Indonesian Seas into the Indian Ocean, and (b) limit ambiguities that can arise from choosing an arbitrary reference salinity and temperature, which is particularly problematic when considering freshwater fractions (Schauer & Losch, 2019).

Volume transport based on observations from the INSTANT program at the Lombok and Ombai straits and in the Timor Sea (2004–2006), and the INSTANT and Monitoring ITF (MITF) programmes at the Makassar Strait (2004–2011) are used to validate the model. A first-order estimate of heat and salt transports based on monthly temperature and salinity profiles from the WOA2018 and the monthly observed current velocities from the INSTANT program are also compared with the model results. The transports at the Lombok and Ombai straits and in the Timor Sea were estimated by laterally and vertically interpolating the observed velocities and assuming a no slip condition at the side-walls of the straits, a zero velocity at the bottom of the Lombok and Ombai straits, and bottom velocities equal to the last observed depth in the Timor Sea. The transports at the Makassar Strait were estimated from the western mooring, as being a representative of the average throughflow across the full width of the Labani Channel following Gordon et al. (2019), by vertically interpolating the observed velocities and assuming zero velocity at the bottom.

3.4.1. Volume Transport

The vertical structure of the volume transport per unit depth reveals flow reversals at different depths and different seasons in the Makassar Strait and the three exit passages of the ITF (Figures 7 and 8). At the Makassar Strait, the southward volume transport per unit depth is largest within the upper 300 m in both the observations and SEAsia-tide (Figure 7a), reflecting the southward current maximum within the upper thermocline (Figure 6a). This upper 300 m transport is strong during boreal summer (July–September) and weak, or even reverses, during boreal winter (November–February) (Figure 7a). This seasonality of the volume transport is due to the freshwater outflow from the Java Sea restricting the southward surface layer flow at the Makassar Strait during winter (Gordon et al., 2012, 2019). Below 300 m, the observed volume transport has a semiannual pattern with reduced southward flow, or weakly reversing flow, during the monsoons transition seasons (April–June and September–November). This flow weakening/reversal is driven by the generation of equatorial Kelvin waves that propagate eastwards and excite coastally-trapped Kelvin waves along the coast of Sumatra, which then penetrate into the Makassar Strait (Pujiana et al., 2013; Sprintall et al., 2000). SEAsia-tide captures this semiannual variability, but slightly overestimates the weakening/reversal of the flow below 300 m (Figure 7a).

SEAsia-tide captures the observed seasonal variability in the volume transport through the Makassar Strait and its minimum during the monsoon transitions (Figure 9a). However, SEAsia-tide simulates a weaker mean transport through the Makassar Strait (9 Sv) than observed (11.6 Sv) that accounts for 61% of the simulated ITF (Table 3). This underestimation of the volume transport mainly occurs at depths below 300 m (Figure 7a).

At the Lombok Strait, the volume transport toward the Indian Ocean is mainly confined within the upper 200 m in the observations and SEAsia-tide (Figure 7b). SEAsia-tide captures the observed seasonal variability of the volume transport through the Lombok Strait, with stronger transport during the southeast monsoon (July–October) (Figure 9b). The flow in the upper 50 m reverses toward the Indonesian Seas during the northwest monsoon (December–March) (Figure 7b), most likely due to locally wind-driven Ekman dynamics (Sprintall et al., 2009). At the Ombai Strait, the seasonal variability in the upper layer volume transport (0–200 m) resembles that at Lombok Strait, with stronger flow toward the Indian Ocean during July–October and flow reversal during December–March (Figure 8a). Weakening or reversal of the flow extending deeper into the water column at the Lombok and Ombai straits is also evident during the monsoon transition in SEAsia-tide and observations (Figures 7b and 8a), driven by propagating coastal Kelvin waves (Sprintall et al., 2000, 2009). Particularly, at the Ombai Strait, the seasonal cycle at depths below 300 m is dominated by this flow reversal, leading to the volume transport being weakest from March to May and from September to November (Figure 9c).

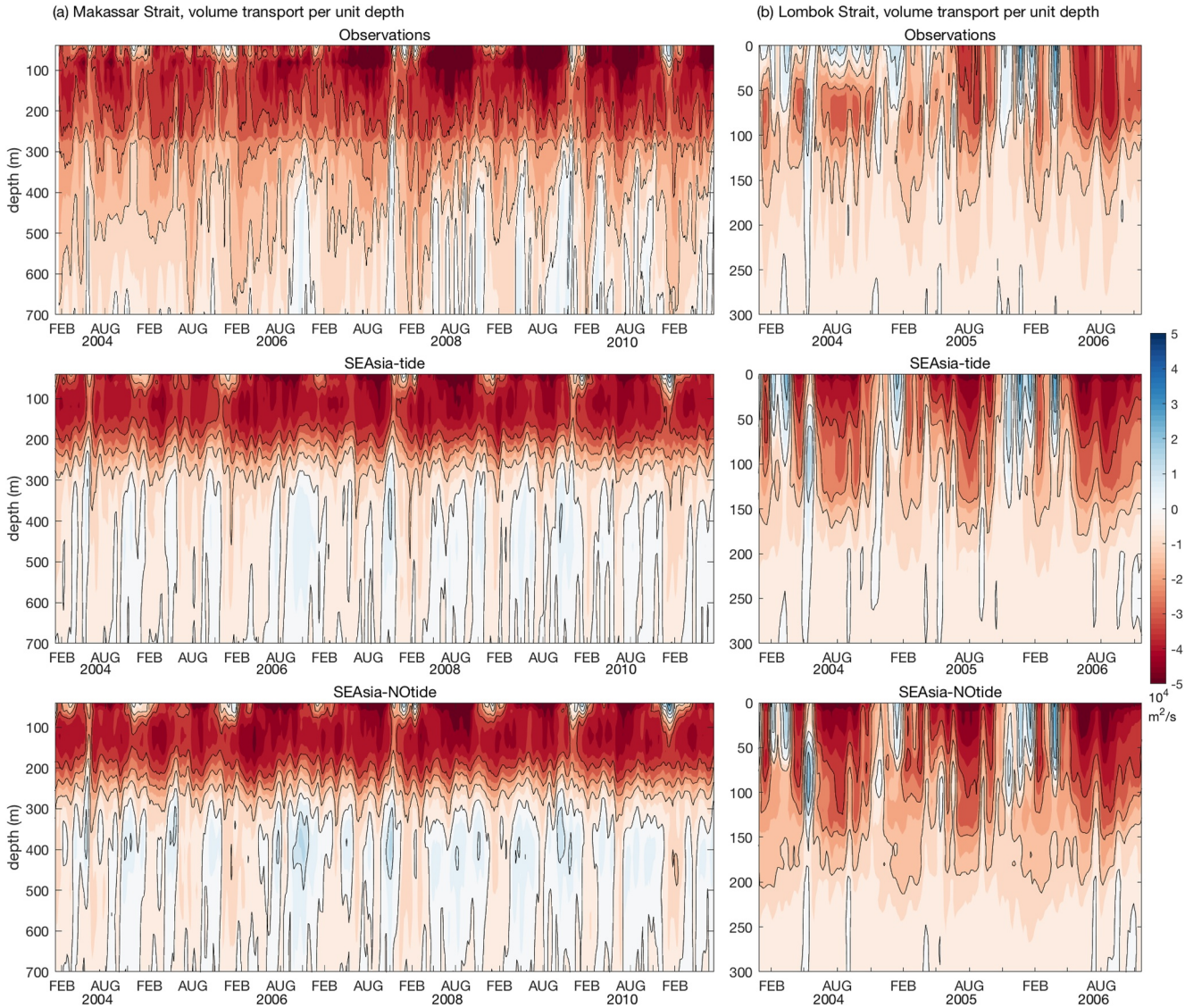

Figure 7. Volume transport per unit depth (10^4 m^{2}s^{-1}): (a) Makassar Strait during 2004–2011, and (b) Lombok Strait during 2004–2006, based on the observations, South East Asia model (SEAsia)-tide and SEAsia-NOtide. The observations are from the International Nusantara Stratification and Transport program (2004–2006) and the Monitoring Indonesian ThroughFlow program (2007–2011) for the Makassar Strait only. A moving average filter of 15 days was applied to the observations and the model results for better visualization. Red color denotes flow toward the Indian Ocean.

In the Timor Sea, the flow reversal toward the Indonesian Seas is more pronounced at greater depths, particularly below 1300 m (Figure 8b). The seasonal cycle of the volume transport in the Timor Sea is out of phase with that at the Ombai Strait (Figures 9c and 9d). In the observations and SEAsia-tide, the volume transport through the Timor Sea reaches its maximum during April–May and its minimum during December–January (Figure 9d). Although, SEAsia-tide captures the observed second peak in the volume transport through the Timor Sea, this peak occurs in September rather than October.

SEAsia-tide has an ITF transport of 14.8 Sv, in good agreement with the observed 15 Sv (Figure 9e and Table 3). SEAsia-tide captures the observed relative partitioning of the transport through the three main exit passages, with the Lombok Strait contributing 2.9 Sv (20%), the Ombai Strait contributing 4.6 Sv (31%) and the Timor Sea contributing 7.3 Sv (49%) to the ITF (Table 3). The ITF transport is only 0.8 Sv weaker in the absence of tides (Table 3). However, in the absence of tides there is a stronger volume transport through the Lombok and Ombai straits but a substantially weaker volume transport through the Timor Sea. Including the tides improves

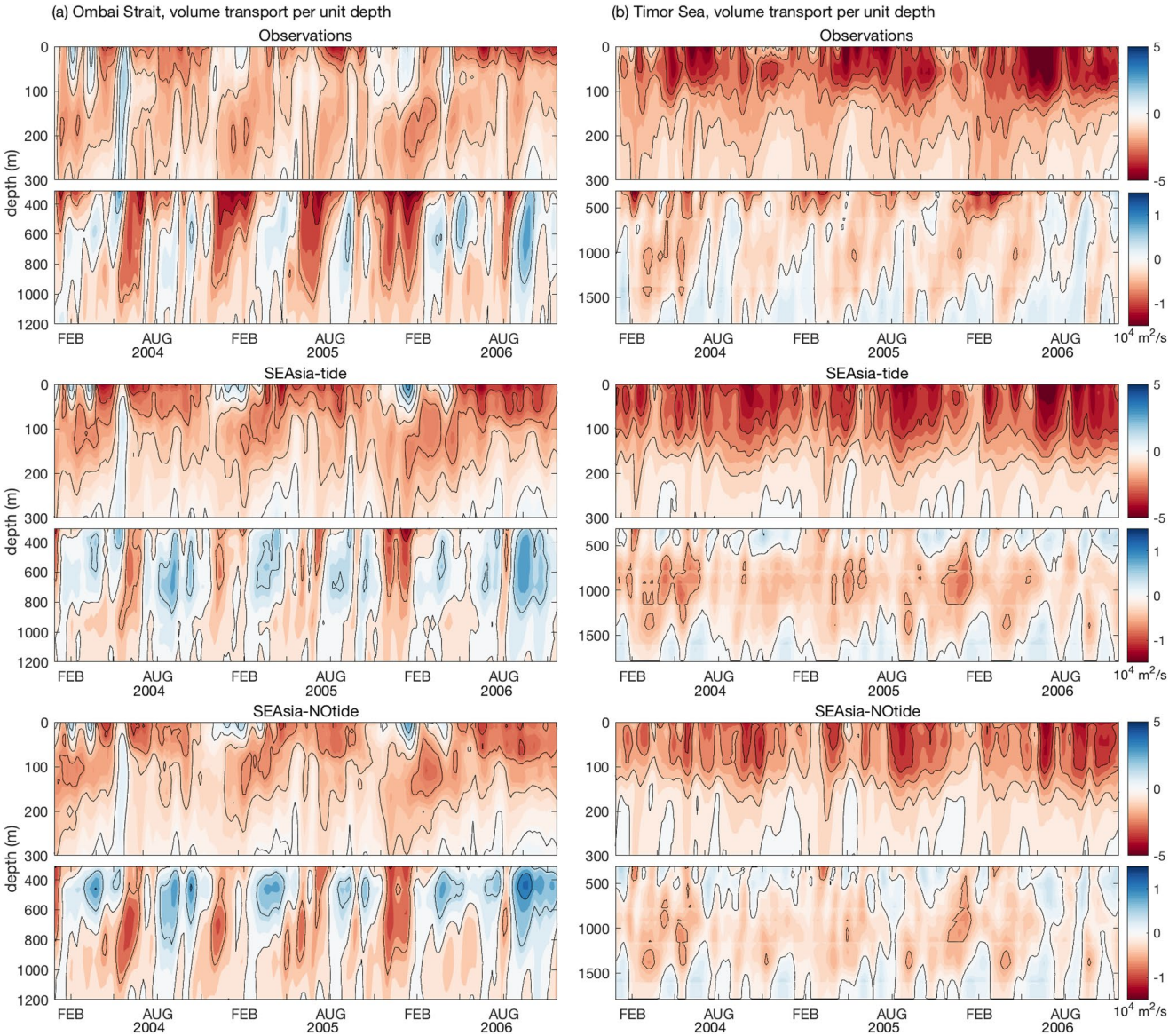

Figure 8. Volume transport per unit depth (10^4 m^{2}s^{-1}): (a) Ombai Strait and (b) the Timor Sea during 2004–2006, based on observations, South East Asia model (SEAsia)-tide and SEAsia-NOtide. The observations are from the International Nusantara Stratification and Transport program. A moving average filter of 15 days was applied to the observations and the model results for better visualization. Red color denotes flow toward the Indian Ocean.

the model's agreement with observations in terms of the ITF volume transport and its fractional contribution of the three main exit passages (Table 3).

In the model, interannual variability in the ITF is associated with the El Niño Southern Oscillation (ENSO) (Figure S8 in Supporting Information S1), as has been suggested by previous studies (England & Huang, 2005; Feng et al., 2018; Gordon et al., 2012; Susanto et al., 2012, 2022; van Sebille et al., 2014). During strong El Niño the ITF weakens by about 2.4 Sv and during La Niña the ITF strengthens by about 1.6 Sv relative to the 1981–2012 mean in both the SEAsia-tide and SEAsia-NOtide (Table 4). El Niño (La Niña) conditions are associated with a decrease (increase) in the volume transport at the Makassar and Ombai straits and in the Timor Sea in the model. In contrast, ENSO has a very limited effect on the volume transport at the Lombok Strait in the model. The similarity in the ITF's link to ENSO between the SEAsia-tide and SEAsia-NOtide (Table 4 and Figure S8 in Supporting Information S1) indicates that the tidal effects on the ITF do not directly depend on the ENSO phase.

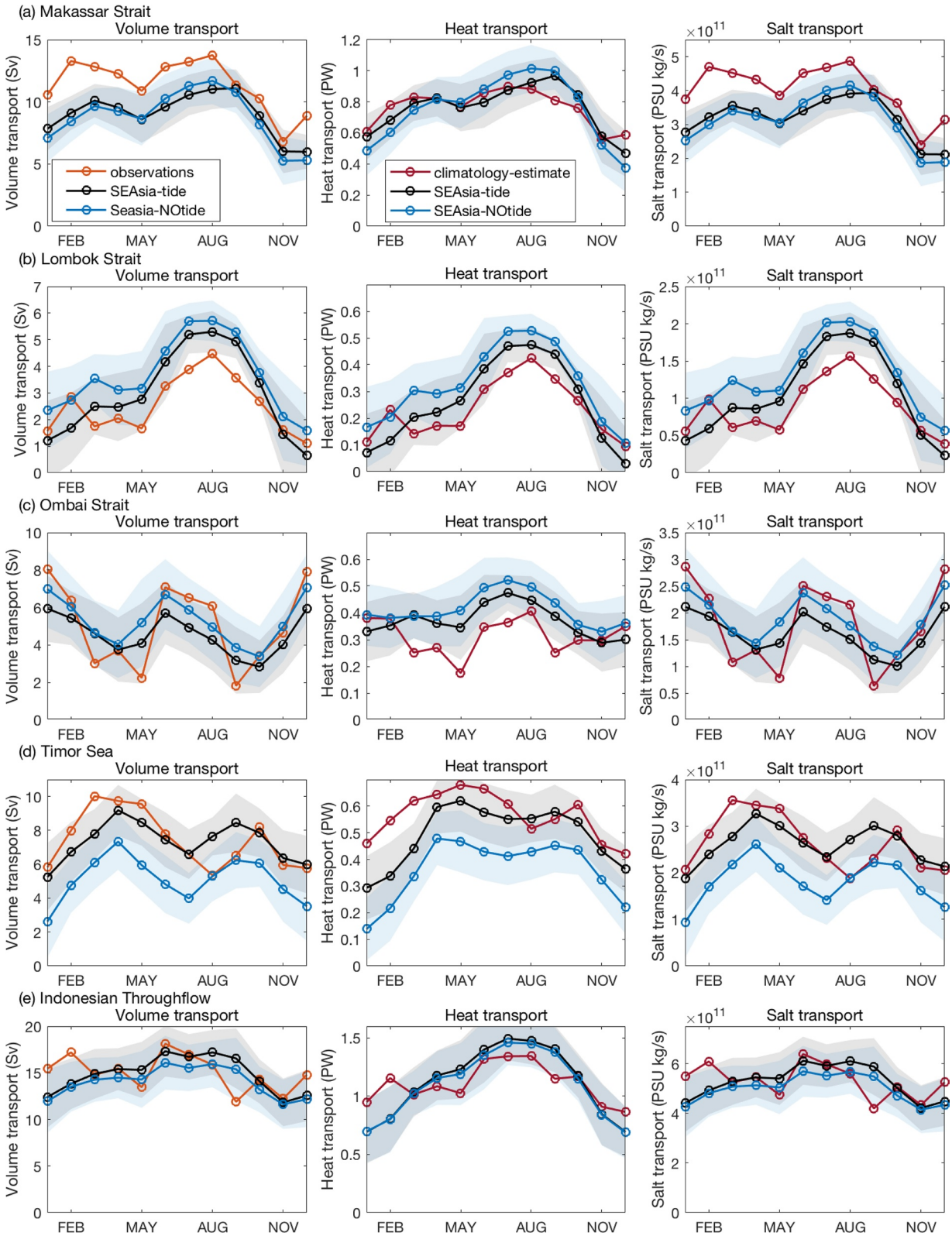
(a) Makassar Strait
Volume transport
Heat transport
Salt transport
Volume transport (Sv)
Heat transport (PW)
Salt transport (PSU kg/s)
observations
SEAsia-tide
Seasia-NOtide
climatology-estimate
SEAsia-tide
SEAsia-NOtide
(b) Lombok Strait
(c) Ombai Strait
(d) Timor Sea
(e) Indonesian Throughflow
FEB
MAY
AUG
NOV

Figure 9.

Table 3
Volume Transport (Sv) Estimates Associated With the Indonesian Throughflow From Observations, South East Asia Model (SEAsia)-tide and SEAsia-NOtide

	Observations	SEAsia-tide	SEAsia-NOtide
Makassar Strait	11.6 (8.3–14.9), 77%	9.0 ± 0.9, 61%	8.8 ± 1.0, 63%
Lombok Strait	2.6 (1.8–3.2), 17%	2.9 ± 0.4, 20%	3.6 ± 0.4, 26%
Ombai Strait	4.9 (2.7–5.0), 33%	4.6 ± 0.8, 31%	5.3 ± 0.9, 38%
Timor Sea	7.5 (6.2–10.5), 50%	7.3 ± 0.7, 49%	5.1 ± 0.7, 36%
ITF	15.0 (10.7–18.7)	14.8 ± 1.5	14 ± 1.6

Note. The observations are based on the INSTANT program (2004–2006). The model estimates are based on years 1981–2012. The observations uncertainty is shown within the parentheses and the model interannual variability is shown as ± one standard deviation. The ITF is estimated as the combined volume transport from the Lombok, Ombai and Timor exit passages. The fractional contribution of each of the three exit passages to the ITF is also shown as a percentage.

3.4.2. Heat and Salt Transports

SEAsia-tide simulates a heat transport (referenced to 0°C) through the Makassar strait in good agreement with previous studies (Vranes et al., 2002) and the first-order estimate from climatology, both in terms of magnitude and seasonal variability (Table 5 and Figure 9a). The heat transport weakening at the Makassar Strait during May and during November–January is mainly due to a lower volume transport (Figure 9a). SEAsia-tide also simulates the seasonal variability in heat transport through the Lombok, Ombai and Timor exit passages, although it has a less pronounced seasonal cycle at the Ombai Strait than the first-order estimate from climatology (Figures 9b–9d). SEAsia-tide overestimates the heat transport by 0.03 PW at the Lombok Strait and by 0.06 PW at the Ombai Strait, but underestimates it by 0.07 PW in the Timor Sea (Table 5). SEAsia-tide has an ITF heat transport of 1.12 PW, in good agreement with the climatology-based estimate of 1.10 PW (Table 5). The Lombok Strait, Ombai Strait and the Timor Sea contribute 23%, 33% and 44%, respectively, to the ITF heat transport in SEAsia tide, which is in reasonable agreement to the estimates based on climatology (Table 5).

The seasonal variability in the salt transport (referenced to 0 PSU) reflects that of the volume transport (Figure 9). At the Makassar Strait, SEAsia-tide robustly captures the seasonal variability in the salt transport, with weakening during May and November–January (Figure 9a), but underestimates it by 0.8×10^{11} PSU kg s^{-1} relative to the first-order estimate based on climatology (Table 5). SEAsia-tide overestimates the salt transport by 0.1×10^{11} PSU kg s^{-1} at the Lombok Strait, but underestimates it by 0.2×10^{11} PSU kg s^{-1} at the Ombai Strait (Table 5). Hence, the ITF salt transport is only slightly lower (0.1×10^{11} PSU kg s^{-1}) in the SEAsia-tide relative to the estimates based on climatology (Table 5).

In SEAsia-NOtide the ITF heat and salt transports (1.10 PW and 5.0×10^{11} PSU kg s^{-1}, respectively) are only slightly weaker than in SEAsia-tide (Table 5). However, this overall agreement between SEAsia-tide and SEAsia-NOtide is somewhat misleading, as in the absence of tides the heat and salt transports increase at the Lombok and Ombai straits, but decrease by about 0.1 PW and 0.8×10^{11} PSU kg s^{-1} in the Timor Sea (Table 5).

4. Effect of Tides on the Indonesian Throughflow: Contribution From Different Processes

4.1. Effect of Tides on Water Mass Transformation Within the Indonesian Seas

Within the Indonesian Seas there is strong generation of baroclinic tides due to the interaction between tides and complex topography in water that is stratified. These waves are trapped within these semi-enclosed seas and dissipate locally (Koch-Larrouy et al., 2007; Nagai & Hibiya, 2015; Nugroho et al., 2018). This generation and dissipation of baroclinic tides leads to a strong vertical mixing that contributes to the water mass transformation within the Indonesian Seas (Gordon, 2005; Koch-Larrouy et al., 2008; Robertson & Ffield, 2005, 2008). To isolate this effect of mixing due to tides on temperature and salinity, the total tracer (i.e., salinity or temperature), C, is separated into two terms, such that

$$\overline{C} = \overline{C_{\text{back}}} + \underbrace{\overline{C_{\text{inter}}}}_{\text{effect of tides}}, \tag{4}$$

where the overbar denotes time-averaged, C_{back} is the background tracer driven by the atmospheric forcing, the ocean forcing imposed at the model's open lateral boundaries and the rivers runoff, and C_{inter} is the tracer driven

Figure 9. Volume, heat and salt transports: (a) Makassar Strait, (b) Lombok Strait, (c) Ombai Strait, (d) the Timor Sea and (e) Indonesian Throughflow, based on observations, South East Asia model (SEAsia)-tide and SEAsia-NOtide. The observed volume transport estimates are based on current observations from the International Nusantara Stratification and Transport program (2004–2006) and the Monitoring Indonesian ThroughFlow program (2007–2011) for the Makassar Strait only. The first order climatology estimates for the heat and salt transports are based on monthly-averaged observed currents and monthly-averaged temperature and salinity from the World Ocean Atlas climatology. The estimates based on the SEAsia model are based on 5-day averaged currents, temperature and salinity during years 1981–2012. The heat and salt transport are estimated based on a referenced temperature and salinity of 0°C and 0 PSU, respectively. The solid lines show the model mean and the shading the model variability as one standard deviation during years 1981–2012.

Table 4
Average Volume Transport (Sv) Associated With the Indonesian Throughflow From the South East Asia Model (SEAsia)-tide and SEAsia-NOtide for Years 1981–2012, for Strong El Niño Years (1982–1983, 1987–1988, 1991–1992, 1997–1998, 2009–2010) and for Strong La Niña Years (1988–1989, 1998–2000, 2007–2008, 2010–2011)

SEAsia-tide (SEAsia-NOtide)			
	Years 1981–2012	El Nino years	La Nina years
Makassar Strait	9.0 (8.8)	8.1 (7.6)	9.6 (9.5)
Lombok Strait	2.9 (3.6)	3.0 (3.6)	2.8 (3.5)
Ombai Strait	4.6 (5.3)	3.2 (3.8)	5.4 (6.3)
Timor Sea	7.3 (5.1)	6.2 (4.1)	8.2 (5.9)
ITF	14.8 (14.0)	12.4 (11.5)	16.4 (15.7)

Note. The ITF is estimated as the combined volume transport from Lombok, Ombai and Timor exit passages. The SEAsia-NOtide is shown inside the parentheses.

by the interaction between the barotropic tide and the density gradient (i.e., tidal-mixing). The terms in Equation 4 are estimated based on the SEAsia model experiments (Table 1) as shown in Table 6.

Tidal mixing erodes the stratification of the Pacific water within the Indonesian Seas leading to a more well-mixed water mass (Figures 3a and 3b). At the western path of the ITF, in the Celebes Sea and Makassar Strait, tides lead to a gradual freshening and cooling of the thermocline at the expense of warming at depth and an increase in the salinity at the surface and intermediate depths (Figures 10a and 10c). East of the Flores Sea, tides lead to a freshening of the surface layer (Figure 10a) due to a wind-driven coastal upwelling along the north of the Lesser Sunda Islands bringing upper thermocline water to the surface that is well-mixed and relatively fresh; in contrast, in the simulations without tides this upwelling water is more saline. At the eastern path of the ITF, in the Halmahera Sea, tides lead to pronounced warming below 500 m but large freshening between about 100 and 400 m; which reflects the erosion of the South Pacific subtropical water by tidal mixing before entering the Banda Sea (Figures 10b and 10d). The signature of this freshening reaches down to 500 m east of the Flores Sea and within the Banda Sea (Figures 10a and 10b).

At the Makassar, Lombok and Ombai straits and in the Timor Sea the background salinity (i.e., with no tidal mixing) has an unrealistic vertical structure reflecting a clear signature of Pacific subtropical and intermediate waters (Figure 10e). In the absence of tides a salinity maximum of about 34.8 PSU, associated with the North Pacific Subtropical water, is retained within the thermocline throughout the Makassar, Lombok and Ombai straits (Figure 10e). In the Timor Sea, the background salinity within the thermocline reaches as high as 35 PSU due to the influence of South Pacific Subtropical water that has experienced limited mixing before reaching the Timor Sea in the absence of tides. The tidal mixing generally cools the surface and upper layer and brings heat down to greater depths (Figure 10e). Overall, in all the exit passages of the ITF, tides drive a decrease in temperature and

Table 5
Heat Transport (PW) and Salt Transport (PSU kg s^{-1}) Associated With the Indonesian Throughflow in Absolute Terms (i.e., Relative to 0°C and 0 PSU), From Climatology-Based Estimates, South East Asia Model (SEAsia)-tide and SEAsia-NOtide

Heat transport relative to 0°C (PW)			
	Climatology	SEAsia-tide	SEAsia-NOtide
Makassar Strait	0.76, 69%	0.76 ± 0.08, 68%	0.75 ± 0.08, 68%
Lombok Strait	0.23, 21%	0.26 ± 0.04, 23%	0.33 ± 0.04, 30%
Ombai Strait	0.31, 28%	0.37 ± 0.05, 33%	0.41 ± 0.05, 37%
Timor Sea	0.56, 51%	0.49 ± 0.06, 44%	0.36 ± 0.06, 33%
ITF	1.10	1.12 ± 0.12	1.10 ± 0.13
Salt transport relative to 0 PSU (10^{11} PSU kg s^{-1})			
	Climatology	SEAsia-tide	SEAsia-NOtide
Makassar Strait	4.0, 75%	3.2 ± 0.3, 62%	3.1 ± 0.4, 62%
Lombok Strait	0.9, 19%	1.0 ± 0.2, 19%	1.3 ± 0.2, 26%
Ombai Strait	1.8, 32%	1.6 ± 0.3, 31%	1.9 ± 0.3, 38%
Timor Sea	2.6, 49%	2.6 ± 0.2, 50%	1.8 ± 0.2, 36%
ITF	5.3	5.2 ± 0.5	5.0 ± 0.6

Note. The climatology-based estimates are based on monthly averaged volume transports from the INSTANT program (2004–2006) and temperature and salinity from the World Ocean Atlas (1981–2010 period). The model estimates are based on years 1981–2012. The model interannual variability is shown as ± one standard deviation. The ITF is estimated as the combined transports from the Lombok, Ombai and Timor exit passages. The fractional contribution of each of the three exit passages to the ITF is also shown as a percentage.

Table 6
Combination of the Three South East Asia Model Experiments (Table 1) Used to Estimate the Different Terms for the Tracer in Equation 4 and Current in Equation 5

	Term in Equations 4 and 5	Experiments used
Total tracer	C	SEAsia-tide
Background tracer	C_{back}	SEAsia-NOtide
Effect of tides on tracer	C_{inter}	(SEAsia-tide) − (SEAsia-NOtide) (i.e., $C - C_{\text{back}}$)
Total current	$\mathbf{u}$	SEAsia-tide
Background current	$\mathbf{u}_{\text{back}}$	SEAsia-NOtide
Barotropic tidal current	$\mathbf{u}_{\text{BTtide}}$	SEAsia-BTtide
Current due to interaction	$\mathbf{u}_{\text{inter}}$	(SEAsia-tide) − (SEAsia-NOtide + SEAsia-BTtide) (i.e., $\mathbf{u} - \mathbf{u}_{\text{back}} - \mathbf{u}_{\text{BTtide}}$)

Note. The current due to interaction refers to the current driven by the interaction between tides and stratification.

salinity in the upper thermocline and an increase at depths below 600 m (Figure 10e), reflecting vertical mixing of the water masses.

4.2. Effect of Tides on the Indonesian Seas Circulation

Tides affect the ocean circulation through the interaction of barotropic tide with topography generating residual currents (Huthnance, 1973; Loder, 1980; Polton, 2015). These barotropic tidal residual currents are further modified by internal friction due to stratification (Wright & Loder, 1985). Tides also indirectly affect the ocean currents through their interaction with stratification generating baroclinic tides that can enhance mixing, modify the density gradient and so alter the general circulation.

To investigate the effect of tides on the mean circulation, the current, $\mathbf{u}$, is split into contributions from three terms, such that

$$\overline{\mathbf{u}} = \overline{\mathbf{u}_{\text{back}}} + \underbrace{\overline{\mathbf{u}_{\text{BTtide}}} + \overline{\mathbf{u}_{\text{inter}}}}_{\text{effect of tides}}, \tag{5}$$

where the overbar denotes time-averaged (equivalent to a residual in terms of the effect of tides), $\mathbf{u}_{\text{back}}$ is the background current driven by the atmospheric forcing, the ocean forcing imposed at the model's open lateral boundaries and the rivers runoff, $\mathbf{u}_{\text{BTtide}}$ is the current driven solely by the barotropic tide and its interaction with topography, and $\mathbf{u}_{\text{inter}}$ is the current driven by the interaction between tides and stratification. Hence, $\mathbf{u}_{\text{inter}}$ includes (a) the effect of mixing due to the baroclinic tide dissipation on the circulation, and (b) the effect of internal friction due to stratification on the barotropic tidal residual circulation. The combined second and third terms in Equation 5 represent the effect of tides on the mean circulation. The terms in Equation 5 are estimated based on the SEAsia model experiments (Table 1) as shown in Table 6. For simplicity we refer to the first term on the right hand side of Equation 5 as the background current, to the second term on the right hand side of Equation 5 as the barotropic tidal residual current, and to the third term on the right hand side of Equation 5 as the baroclinic tidal residual current.

In SEAsia, tides and their interaction with topography and stratification drive a residual current (0.1 m s^{-1}) that follows the eastern route of the ITF from the Pacific into and around the Banda Sea and then into the Timor Sea, but with significant recirculation in the Molucca Sea (Figure 11a). A tidally induced inflow from the Indian Ocean at the Lombok Strait feeds a residual flow northwards through the Java Sea and through the shallow western side of the Makassar Strait. At the deep eastern side of the Makassar Strait, the tidal residual circulation is southwards along the general direction of the ITF, with this flow continuing eastwards in the Flores Sea and joining the tidal residual flow from the eastern side of the Indonesian Seas (Figure 11a).

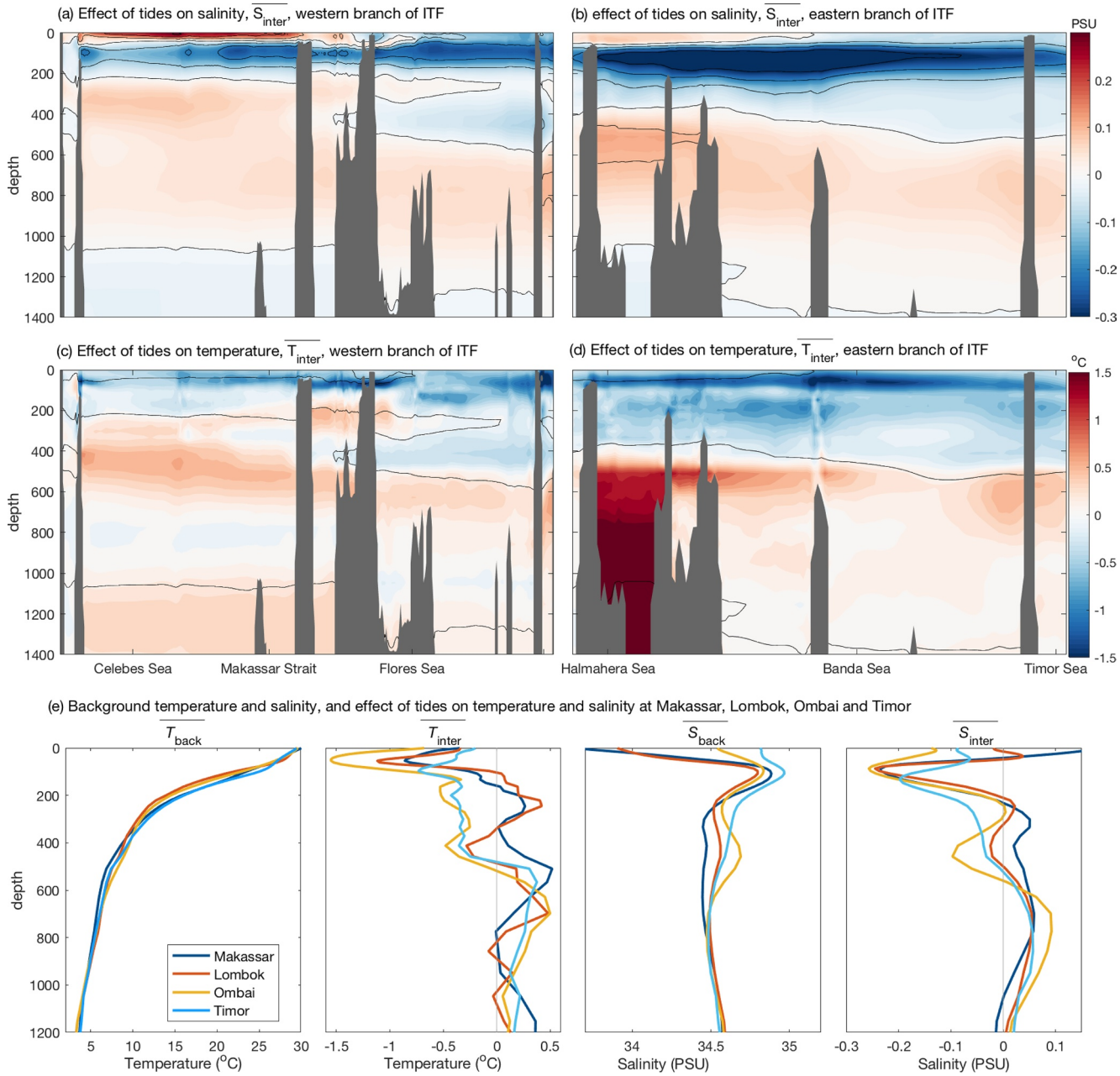

Figure 10. Effect of tides on (a and b) salinity, and (c and d) temperature along two sections through the Indonesian Seas, and (e) background temperature and salinity ($\overline{C_{back}}$ in Equation 4), and effect of tides on temperature and salinity ($\overline{C_{inter}}$ in Equation 4) at Makassar, Ombai and Lombok straits and in the Timor Sea in the South East Asia model. The location of the sections through the Indonesian Seas are shown in the inset-panels in Figures 3a and 3b.

The baroclinic tidal residual is generally larger than the barorotropic tidal residual except over bathymetric features (Figures 11b and 11c, and zoom-in Figures S9 and S10 in Supporting Information S1): at shallow regions (blue arrows), at narrow straits surrounding the Celebes Sea, south of the Makassar Strait, at the Lombok and Ombai straits and north of the Banda Sea. We found a relatively larger tidal residual transport along the eastern route than the western route of the ITF consistent with Hatayama et al. (1996). We also found large tidal residual flow from the Indian Ocean toward the Indonesian Seas at the Lombok Strait in contrast with Schiller (2004). The SEAsia model has a much higher resolution (~9 km) than the model used in Schiller (2004) (~50 km) and so better captures the interaction between barotropic tide topography and stratification at narrow straits.

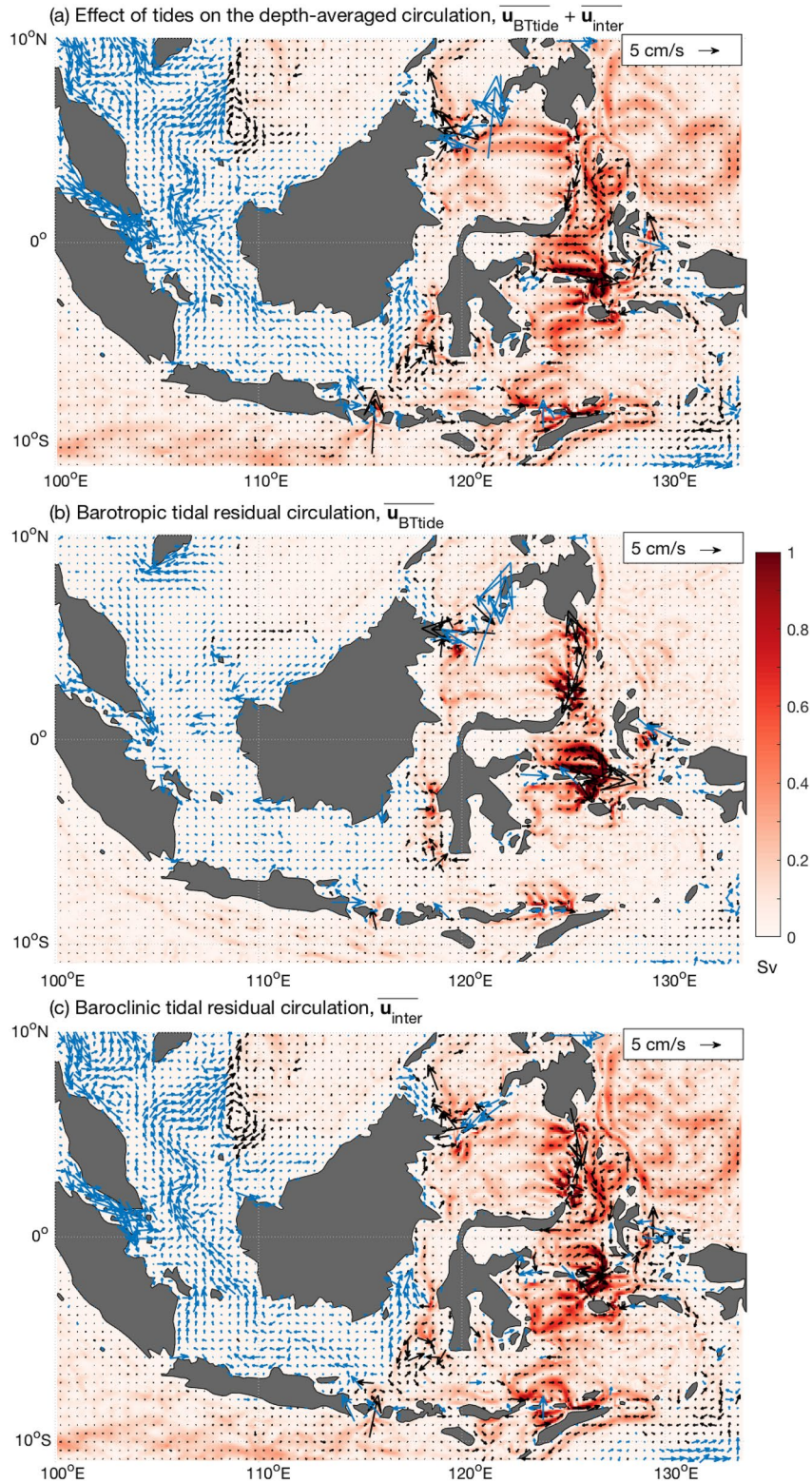

Figure 11. Effect of tides on the depth-averaged circulation in South East Asia model: (a) tidal residual circulation ($u_{\mathrm{BTtide}} + u_{\mathrm{inter}}$ in Equation 5), (b) barotropic tidal residual circulation (u_{BTtide} in Equation 5), and (c) baroclinic tidal residual circulation (u_{inter} in Equation 5). The blue arrows show circulation in regions with bathymetry less than 100 m and the black arrows show circulation in regions with bathymetry deeper than 100 m. The color-scheme shows the magnitude of the volume transport.

Table 7
Effect of Tides on the Volume Transport (Sv) Associated With the Indonesian Throughflow in the South East Asia Model, Along With the Contribution From the Barotropic Tidal Residual Current and the Baroclinic Tidal Residual Current as Described in Equation 6

	Effect of tides	Barotropic tide	Interaction
Makassar Strait	0.22, 2.4%	−0.35, 3.9%	0.57, 6.3%
Lombok Strait	−0.66, 22.8%	−0.08, 2.8%	−0.58, 20%
Ombai Strait	−0.75, 16.3%	−0.29, 6.3%	−0.46, 10.0%
Timor Sea	2.22, 30.4%	0.50, 6.9%	1.72, 23.6%
ITF	0.81, 5.5%	0.13, 0.9%	0.68, 4.6%

Note. The relative fractional change to the volume transport caused by tides is also shown as a percentage. Positive indicates transport toward the Indian Ocean.

4.3. Effect of Tides on the Indonesian Throughflow

4.3.1. ITF Volume Transport

By substituting Equation 5 into Equation 1, the effect of tides to the volume transport associated with the ITF is separated into

$$\underbrace{\overline{\int (u - u_{\text{back}})\, dA}}_{\text{effect of tides}} = \underbrace{\overline{\int u_{\text{BTide}} dA}}_{\text{barotropic tide}} + \underbrace{\overline{\int u_{\text{inter}} dA}}_{\text{interaction}} \tag{6}$$

where the overbar denotes time-averaged, and u is the normal velocity to the area dA. The first term on the right hand side of Equation 6, labeled as "barotropic tide," corresponds to the residual volume transport due to the barotropic tide and its interaction with topography. The second term on the right hand side of Equation 6, labeled as "interaction," corresponds to the residual volume transport due to the interaction between the barotropic tide and the background stratification. For simplicity, we refer to the "interaction" term as the baroclinic tidal residual transport. Here, we consider climatological-monthly volume transports estimated based on 1981–2012. Note that the barotropic tidal residual volume transport is estimated based on a 3 years model run for simplicity, and hence small effects from the long-period tides are ignored.

At the Makassar Strait, the barotropic tide and its interaction with topography leads to a residual transport of 0.35 Sv toward the Pacific Ocean (barotropic tide in Table 7). The baroclinic tidal residual transport (interaction in Table 7) is toward the Indian Ocean and opposes the barotropic tidal residual transport during September–May, but toward the Pacific Ocean and strengthens the barotropic tidal residual transport during June–August (Figure 12a). Hence, at the Makassar Strait the total tidal residual transport has a strong seasonal cycle and leads to an increase in the volume transport toward the Indian Ocean of up to 0.7 Sv during September–May, but to a decrease of up to 0.8 Sv during June–August (Figure 12a). Due to this seasonality of the baroclinic tidal residual transport, on an annual time scale, tides drive only a small increase (0.22 Sv or 2.4%) in the transport of water through the Makassar Strait (Table 7).

At the Lombok Strait, both the barotropic and baroclinic tidal residual transports are from the Indian Ocean toward the Indonesian Seas (Figure 12b). The barotropic tidal residual transport at the Lombok Strait is 0.08 Sv all year round (2.8%, Table 7). The baroclinic tidal residual transport toward the Indonesian Seas is large during winter (about 1 Sv), reducing the total transport of water from the Lombok Strait to the Indian Ocean to half the background transport (Figure 12b). Overall, tides lead to a yearly-averaged reduction of 0.66 Sv (22.8%) in the water transport toward the Indian Ocean from the Lombok Strait.

At the Ombai Strait the barotropic and baroclinic tidal residual transports are of similar magnitude and generally act to decrease the volume transport toward the Indian Ocean (Figure 12c). However, in March the baroclinic tidal residual transport weakly reverses, which leads to the overall effect of tides on the volume transport to be negligible at the Ombai Strait during this period. Overall, tides lead to a decrease of 0.75 Sv (16.3%) in the volume transport toward the Indian Ocean at the Ombai Strait (Table 7).

In the Timor Sea, tides drive an increase in the volume transport toward the Indian Ocean, in contrast to the Ombai and Lombok straits (Figure 12d). The barotropic tide leads to a residual transport of 0.5 Sv toward the Indian Ocean in the Timor Sea (Table 7). The interaction between barotropic tide and background stratification leads to a residual transport toward the Indian Ocean that reaches more than 2 Sv in January and July, but reduces down to 1 Sv during the monsoon transition (Figure 12d). The combined barotropic and baroclinic tidal residual volume transport toward the Indian Ocean is 2.22 Sv, or equivalently 30% of the total flow at the Timor passage.

In terms of the ITF, tides contribute only to a 0.81 Sv (5.5%) increase, with the barotropic tide driving a 0.13 Sv increase all year round and the interaction between the barotropic tide and background stratification driving a 0.68 Sv mean increase that intensifies during summer (Figure 12e and Table 7). This apparently small contribution from tides to the ITF is due to a compensation between the relatively large but opposing tidal residual transports at the three main exit passages: (a) a 1.4 Sv tidal residual transport toward the Indonesian Seas at the

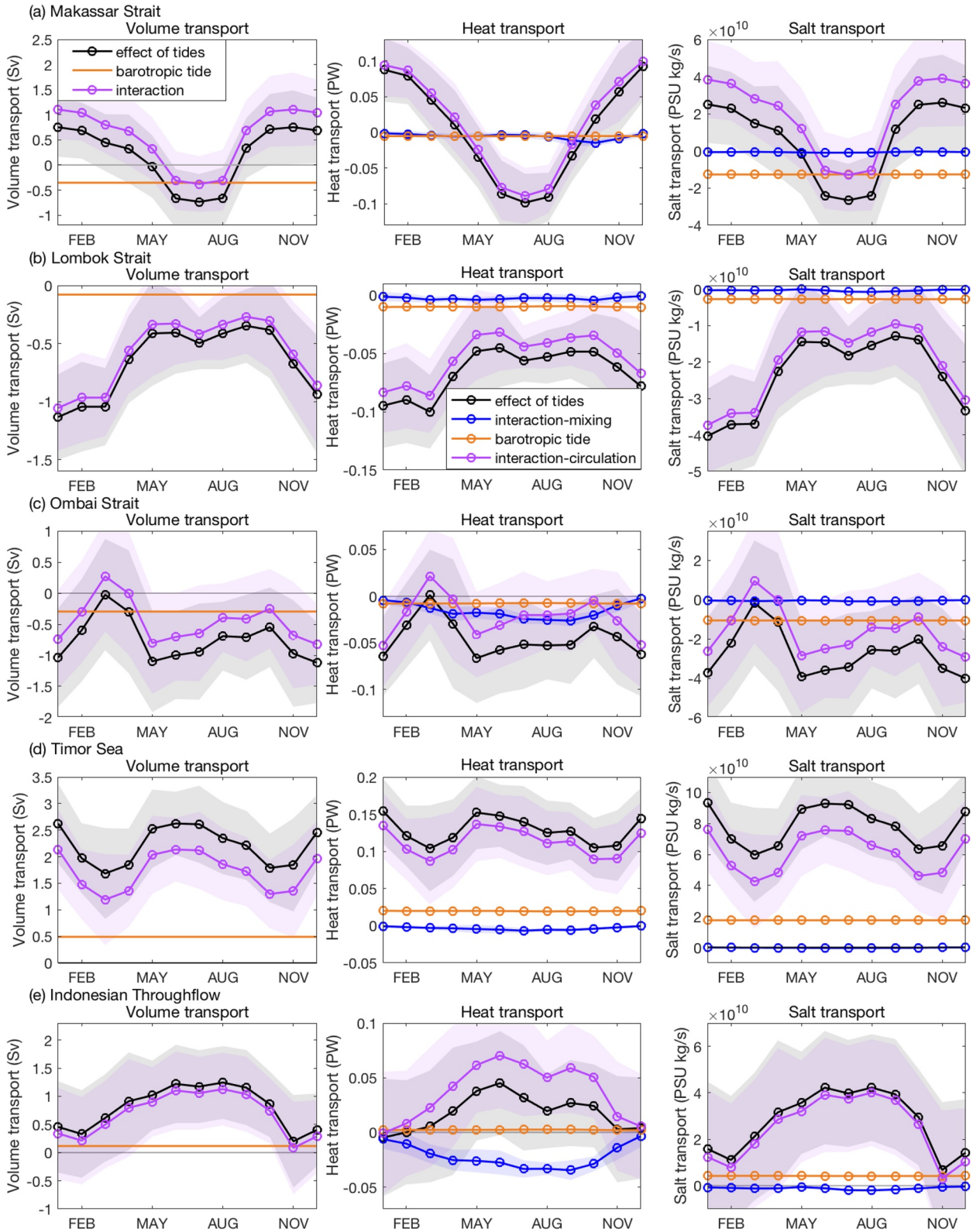
(a) Makassar Strait
Volume transport
Heat transport
Salt transport
effect of tides
barotropic tide
interaction
Volume transport (Sv)
Heat transport (PW)
Salt transport (PSU kg/s)
×10^10
FEB
MAY
AUG
NOV
(b) Lombok Strait
effect of tides
interaction-mixing
barotropic tide
interaction-circulation
(c) Ombai Strait
(d) Timor Sea
(e) Indonesian Throughflow

Figure 12.

combined Ombai and Lombok straits, and (b) a 2.2 Sv tidal residual transport toward the Indian Ocean in the Timor Sea.

4.3.2. ITF Heat and Salt Transports

The effect of tides on the transport of a tracer (e.g., heat and salt) can be expressed by combining Equations 1, 4, and 5 as

$$\underbrace{\overline{\int (C \cdot u - C_{\text{back}} \cdot u_{\text{back}})\, dA}}_{\text{effect of tides}} = \overline{\int ((C_{\text{inter}} \cdot u_{\text{back}}) + (C_{\text{back}} + C_{\text{inter}}) \cdot (u_{\text{BTtide}} + u_{\text{inter}}))\, dA}$$
$$= \underbrace{\overline{\int C_{\text{inter}} \cdot u_{\text{back}} dA}}_{\text{interaction-mixing}} + \underbrace{\overline{\int C \cdot u_{\text{BTtide}} dA}}_{\text{barotropic tide}} + \underbrace{\overline{\int C \cdot u_{\text{inter}} dA}}_{\text{interaction-circulation}} \quad (7)$$

where the overbar denotes time-averaged, u is the normal velocity to the area dA and C is the tracer. The first term on the right hand side in Equation 7, labeled as "interaction-mixing," corresponds to the tracer transport due to the background current carrying the changes in tracer due to tidal mixing. The second term on the right hand side in Equation 7, labeled as "barotropic tide," corresponds to the tracer transport due to the barotropic tidal residual current carrying the total tracer. The third term on the right hand side in Equation 7 labeled as "interaction-circulation," corresponds to the tracer transport due to the baroclinic tidal residual current carrying the total tracer. Substituting either $c_p\rho\theta$ or ρS to C in Equation 7 provides the expression for the effect of tides on the heat and salt transports. Note that the tracer transport estimates are based on 5-day mean model outputs and so we ignore the contribution from higher frequency correlations between current and tracer.

The effect from the baroclinic tidal residual current (i.e., interaction-circulation term) dominates the influence of tides to the "absolute" heat and salt transports (i.e., referenced to 0°C and 0 PSU) at the Makassar, Lombok and Ombai straits and in the Timor Sea; while the effect from tidal mixing on temperature and salinity (i.e., interaction-mixing term) has the smallest contribution (Figure 12). In all the straits, the effect of tidal mixing on temperature and salinity (i.e., interaction-mixing) decreases the heat and salt transports toward the Indian Ocean (Figure 12 and Table 8), as it acts to freshen and cool the upper 300 m (Figure 10) where most of the Indonesia Throughflow takes place (Figures 7 and 8). This effect of the interaction-mixing leads to a decrease of 0.02 PW and 0.01 $\times 10^{11}$ PSU kg s^{-1} in the ITF's heat and salt transports, respectively (Table 8).

In contrast, the barotropic and baroclinic tidal residual currents are either toward the Pacific Ocean or toward the Indian Ocean (Section 4.3.1 and Table 7) and so act to either decrease or increase the heat and salt transports toward the Indian Ocean at the different exit passages (barotropic tide and interaction-circulation terms in Figure 12). At the combined Lombok and Ombai straits the barotropic tidal residual current drives a decrease in the heat and salt transports toward the Indian Ocean of 0.018 PW and 0.14 $\times 10^{11}$ PSU kg s^{-1} (barotropic tide in Table 8), while the baroclinic tidal residual current drives a decrease of 0.076 PW and 0.37 $\times 10^{11}$ PSU kg s^{-1} (interaction-circulation in Table 8). In contrast, in the Timor Sea the barotropic and baroclinic tidal currents drive an increase in the heat transport (0.020 and 0.113 PW) and the salt transport (0.18 $\times 10^{11}$ and 0.61 $\times 10^{11}$ PSU kg s^{-1}) toward the Indian Ocean.

Tides drive modest heat and salt transports from the Indonesian Seas into the Indian Ocean (0.017 PW and 0.27 $\times 10^{11}$ PSU kg s^{-1}). However, this apparently small contribution from tides to the ITF's heat and salt transports involves: (a) a compensation between a large decrease from the barotropic and baroclinic tidal residual currents at the Lombok and Ombai straits and a large increase from these currents in the Timor Sea, and (b) an opposition between the effects from changes in the circulation due to tides and from changes in temperature and salinity distribution due to tidal mixing.

Figure 12. Effect of tides on the volume, heat and salt transports: (a) Makassar Strait, (b) Lombok Strait, (c) Ombai Strait, (d) the Timor Sea and (e) Indonesian Throughflow in the South East Asia model. The effect of tides is separated into contribution from different processes, as described by the terms in Equation 6, for the left column, and in Equation 7, for the middle and right columns. The estimates are based on 5-day averaged currents, temperature and salinity during years 1981–2012. The heat and salt transports are estimated based on a referenced temperature and salinity of 0°C and 0 PSU, respectively. The solid lines show the model mean and the shading the model variability as one standard deviation during years 1981–2012.

Table 8
Effect of Tides on the Heat Transport (PW) and Salt Transport (PSU kg s^{-1}) Associated With the Indonesian Throughflow in Absolute Terms (i.e., Relative to 0°C and 0 PSU) in the South East Asia Model, Along With the Contribution From the Different Terms in Equation 7

Heat transport relative to 0°C (PW)				
	Effect of tides	Interaction-mixing	Barotropic tide	Interaction-circulation
Makassar Strait	0.005, 0.7%	−0.005, 0.7%	−0.005, 0.7%	0.015, 2.1%
Lombok Strait	−0.067, 25.8%	−0.003, 1.2%	−0.010, 3.8%	−0.054, 20.8%
Ombai Strait	−0.045, 12.2%	−0.015, 4.1%	−0.008, 2.2%	−0.022, 5.9%
Timor Sea	0.129, 26.3%	−0.004, 0.8%	0.020, 4.1%	0.113, 23.0%
ITF	0.017, 1.5%	−0.022, 2.0%	0.002, 0.2%	0.037, 3.3%
Salt transport relative to 0 PSU (10^{11} PSU kg s^{-1})				
	Effect of tides	Interaction-mixing	Barotropic tide	Interaction-circulation
Makassar Strait	0.07, 2.1%	−0.01, 0.3%	−0.13, 4.1%	0.21, 6.5%
Lombok Strait	−0.25, 25.0%	−0.00, 0.0%	−0.04, 4.0%	−0.21, 21.0%
Ombai Strait	−0.27, 16.9%	−0.01, 0.6%	−0.10, 6.3%	−0.16, 10.0%
Timor Sea	0.79, 30.4%	−0.00, 0.0%	0.18, 6.9%	0.61, 23.5%
ITF	0.27, 5.2%	−0.01, 0.2%	0.04, 0.8%	0.24, 4.6%

Note. The relative fractional change to the heat and salt transports caused by tides is also shown as a percentage. Positive indicates transport toward the Indian Ocean.

5. Discussion and Summary

In this study, we explored the tidal effects on the transports of water, heat and salt from the Pacific into the Indian Ocean through the Indonesian Seas (i.e., ITF) using a 1/12th degree ocean model of the South East Asia region (SEAsia model). Our SEAsia model captures the observed water masses and circulation within the Indonesian Seas and the ITF, in terms of climatological annual means and seasonality. Our model experiments confirm that tidally-induced mixing plays a key role in the transformation of the Pacific water within the Indonesian Seas into a relatively well-mixed, cool and fresh water mass, as has been suggested by previous studies (Ffield & Gordon, 1996; Kartadikaria et al., 2011; Kida & Wijffels, 2012; Koch-Larrouy et al., 2007, 2008; Nagai & Hibiya, 2015; Nugroho et al., 2018; Ray & Susanto, 2016; Robertson & Ffield, 2008; Tranchant et al., 2016). Hence, tides lead to a more accurate representation of this fresh water mass spreading westewards into the Indian Ocean within the upper thermocline and becoming saltier as it mixes with surrounding waters. Tides also lead to a more realistic circulation in the SEAsia model, particularly in terms of the representation of the observed current reversals toward the Indonesian Seas (Sprintall et al., 2009) along the Lombok, Ombai and Timor exit passages.

The SEAsia model with tides simulates an ITF transport of 14.8 Sv, in good agreement with the observed transport of 15 Sv (Sprintall et al., 2009), and ITF heat and salt transports (referenced to 0°C and 0 PSU) of 1.12 PW and 5.2×10^{11} PSU kg s^{-1}, respectively, in good agreement with our climatology-based estimates. SEAsia with tides also captures the observed relative partitioning of these transports through the three main exit passages, with about 20%, 30% and 50% of the ITF passing through the Lombok Strait, Ombai Strait and Timor Sea, respectively. Tides drive only a modest increase in the ITF volume (0.8 Sv), heat (0.02 PW) and salt (0.3×10^{11} PSU kg s^{-1}) transports in our model. However, tides drive large regional changes to the transports associated with the ITF, and alter the relative contribution from each of the three exit passages to the ITF.

The tidal effects on the ITF were further separated into contributions: (a) from the direct effect of the barotropic tide on the residual circulation through its interaction with topography (i.e., barotropic tidal residual current); (b) from the effect of the interaction between barotropic tide and background stratification to the residual circulation, including the effects of mixing due to the baroclinic tide dissipation on the circulation and of internal friction due to stratification on the barotropic tidal circulation (i.e., interaction-circulation); and (c) from the effect of tidal mixing on the salinity and temperature profiles within the Indonesian Seas (i.e., interaction-mixing). Our SEAsia model experiments indicate that the largest contribution to the impact of tides on the ITF transports comes from the residual circulation driven by the interaction between barotropic tide and background stratification (i.e.,

interaction-circulation). This baroclinic tidal residual circulation drives large but compensatory transports at the different exit passages: transports toward the Indonesian Seas at the Lombok and Ombai straits, but toward the Indian Ocean in the Timor Sea. The barotropic tidal residual circulation is locally large, and at the Ombai Strait its effect on the volume, heat and salt transports is of similar magnitude to that of the baroclinic tidal residual circulation, and even exceeds it during March and October. While the effect of the tidal residual circulation (from the barotropic tide and the interaction-circulation) on the heat and salt transports at the combined Lombok and Ombai straits and in the Timor Sea oppose each other, the changes in salinity and temperature due to tidal mixing (i.e., interaction-mixing) act cumulatively at these three exit passages to decrease the ITF heat and salt transports toward the Indian Ocean by 0.02 PW and 0.01×10^{11} PSU kg s^{-1}, respectively.

Our inferences for the effect of tides on the ITF are based on simulations. The agreement between our model simulations with explicit tidal forcing and observations, particularly in terms of the ITF transport and its partitioning to the Lombok, Ombai and Timor exit passages, provide confidence in our results; although quantitative details in terms of mixing, tidal residual currents and baroclinic tide propagation and dissipation are model and resolution dependent. Our simulations neglect additional effects of tides on the water masses transformation and circulation outside our model domain such as within the Pacific Ocean. These additional effects can further modify the ITF through, for example, changes in the sea surface height gradient between the Pacific and Indian Ocean as shown in Sasaki et al. (2018).

In summary, and returning to the hypotheses posed in the Introduction, tides appear to drive less than 6% of the volume, heat and salt transports associated with the ITF. However, our study reveals that regionally, tides decrease these transports from the Indonesian Seas toward the Indian Ocean by 23%–26% at the Lombok Strait and by 12%–17% at the Ombai Strait, but increase them by 26%–30% in the Timor Sea. Hence, the apparent small effect of tides on the ITF is misleading and due to a compensation of this effect in the different exit passages of the Indonesian Seas. We conclude that tides affect the ITF pathway and control its partitioning to the three main exit passages (Lombok Strait, Ombai Strait and the Timor Sea). The baroclinic tidal residual circulation has the largest contribution in terms of impact of tides to the ITF. However, the barotropic tidal residual circulation is locally significant and drives more than 6% of the water transport at the Ombai Strait and in the Timor Sea.

The effect of tides on the ITF partitioning to the three main exit passages can have implications for the Indian Ocean's physical and biogechemical tracers budgets, as these passages have distinct water characteristics; particularly when comparing the Lombok Strait, where the throughflow consists primarily of upper layer water, with the more eastern passages (Sprintall et al., 2003). For example, an increase in the flow through Lombok Strait at the expense of that through the Timor Sea can lead to a decrease in the salt content of the upper layer within the Indian Ocean since, on average, the upper layer water is fresher at Lombok Strait than in the Timor Sea. Additionally, the ITF supplies nutrients to the Indian Ocean's thermocline, which in turn supports production and affects the biogeochemical cycling within the Indian Ocean; but the amount of this nutrient supply and its depth horizon vary between the Lombok Stait, Ombai Strait and the Timor Sea (Ayers et al., 2014). Hence, tides may regulate the nutrient budget of the Indian Ocean through their effects on the ITF pathway.

Our study indicates that explicit representation of tides is necessary to accurately capture the transport of water from the Pacific Ocean to the Indian Ocean through the Indonesian Seas, particularly in terms of followed pathways. Ocean projections of future climate change rely on Earth system models that do not include tidal forcing. Our results indicate that these models, regardless of their resolution and apparent skill in representing the ITF volume transport (e.g., CMIP5 models, Sen Gupta et al., 2016), may not accurately capture the tracer transports (e.g., heat, salt, nutrients, carbon and pollutants) from the Indonesian Seas into the Indian Ocean.

Data Availability Statement

The output data from the South East Asia model simulations used in this study are available at https://gws-access.jasmin.ac.uk/public/accord/SEAsia_R12/. The repository for this study is at https://github.com/NOC-MSM/SEAsia which contains updated instructions on how to build and run this configuration. The original tagged release for this work is https://github.com/NOC-MSM/SEAsia/releases/tag/v0.0.1. The observations from the International Nusantara Stratification and Transport program and Monitoring Indonesian ThroughFlow programs were downloaded from http://www.marine.csiro.au/~cow074/index.htm and https://academiccommons.columbia.edu/doi/10.7916/d8-p78a-zm51, respectively. The observations from the World Ocean Database, 2018 were

downloaded from https://www.ncei.noaa.gov/products/world-ocean-database and the World Ocean Atlas from https://www.ncei.noaa.gov/access/world-ocean-atlas-2018.

Acknowledgments
This study was supported by the "Addressing Challenges of Coastal Communities through Ocean Research for Developing Economies" (ACCORD) project, which was funded by the Natural Environment Research Council (NERC) as part of Marine National Capability Official Development Assistance and National Capability International Science.

References

Ayers, J. M., Strutton, P. G., Coles, V. J., Hood, R. R., & Matear, R. J. (2014). Indonesian Throughflow nutrient fluxes and their potential impact on Indian Ocean productivity. *Geophysical Research Letters*, *41*(14), 5060–5067. https://doi.org/10.1002/2014GL060593

Bessières, L., Madec, G., & Lyard, F. (2008). Global tidal residual mean circulation: Does it affect a climate OGCM? *Geophysical Research Letters*, *35*(3), L03609. https://doi.org/10.1029/2007GL032644

Boyer, T. P., Baranova, O. K., Coleman, C., Garcia, H. E., Grodsky, A., Locarnini, R. A., et al. (2018). World Ocean Database 2018 [Dataset]. NOAA National Centers for Environmental Information. Retrieved from https://www.ncei.noaa.gov/products/world-ocean-database

Boyer, T. P., García, H. E., Locarnini, R. A., Zweng, M. M., Mishonov, A. V., Reagan, J. R., et al. (2018). World Ocean Atlas 2018 [Dataset]. NOAA National Centers for Environmental Information. Retrieved from https://www.ncei.noaa.gov/access/world-ocean-atlas-2018/

Canuto, V. M., Howard, A., Cheng, Y., & Dubovikov, M. S. (2001). Ocean turbulence. Part I: One-point closure model—Momentum and heat vertical diffusivities. *Journal of Physical Oceanography*, *31*(6), 1413–1426. https://doi.org/10.1175/1520-0485(2001)031<1413:OTPIOP>2.0.CO;2

Dai, A., & Trenberth, K. E. (2002). Estimates of freshwater discharge from continents: Latitudinal and seasonal variations. *Journal of Hydrometeorology*, *3*(6), 660–687. https://doi.org/10.1175/1525-7541(2002)003<0660:EOFDFC>2.0.CO;2

DRAKKAR Group. (2007). Eddy-permitting ocean circulation hindcasts of past decades (Technical report). *CLIVAR-Exchanges*, *12*(3), 8–10.

Dussin, R., Barnier, B., & Brodeau, L. (2016). *Up-dated description of the DFS5 forcing data set: The making of DRAKKAR forcing set DFS5 (DRAKKAR, MyOcean Report)*. LGGE.

England, M. H., & Huang, F. (2005). On the interannual variability of the Indonesian Throughflow and its linkage with ENSO. *Journal of Climate*, *18*(9), 1435–1444. https://doi.org/10.1175/JCLI3322.1

Fang, G., Susanto, R. D., Wirasantosa, S., Qiao, F., Supangat, A., Fan, B., et al. (2010). Volume, heat, and freshwater transports from the South China Sea to Indonesian Seas in the boreal winter of 2007–2008. *Journal of Geophysical Research*, *115*(C12), C12020. https://doi.org/10.1029/2010JC006225

Feng, M., Zhang, N., Liu, Q., & Wijffels, S. (2018). The Indonesian Throughflow, its variability and centennial change. *Geoscience Letters*, *5*(3), 1–10. https://doi.org/10.1186/s40562-018-0102-2

Ffield, A., & Gordon, A. L. (1996). Tidal mixing signatures in the Indonesian Seas. *Journal of Physical Oceanography*, *26*(9), 1924–1937. https://doi.org/10.1175/1520-0485(1996)026<1924:TMSITI>2.0.CO;2

Flather, R. A. (1994). A storm surge prediction model for the northern Bay of Bengal with application to the cyclone disaster in April 1991. *Journal of Physical Oceanography*, *24*(1), 172–190. https://doi.org/10.1175/1520-0485(1994)024<0172:ASSPMF>2.0.CO;2

Gordon, A. L. (2005). Oceanography of the Indonesian Seas and their throughflow. *Oceanography*, *18*(4), 14–27. https://doi.org/10.5670/oceanog.2005.01

Gordon, A. L., & Fine, R. A. (1996). Pathways of water between the Pacific and Indian Oceans in the Indonesian Seas. *Nature*, *379*(6561), 146–149. https://doi.org/10.1038/379146a0

Gordon, A. L., Huber, B. A., Metzger, E. J., Susanto, R. D., Hurlburt, H. E., & Adi, T. R. (2012). South China Sea throughflow impact on the Indonesian Throughflow. *Geophysical Research Letters*, *39*(11), L11602. https://doi.org/10.1029/2012GL052021

Gordon, A. L., Ma, S., Olson, D. B., Hacker, P., Ffield, A., Talley, L. D., et al. (1997). Advection and diffusion of Indonesian Throughflow water within the Indian Ocean South Equatorial Current. *Geophysical Research Letters*, *24*(21), 2573–2576. https://doi.org/10.1029/97GL01061

Gordon, A. L., Napitu, A., Huber, B. A., Gruenburg, L. K., Pujiana, K., Agustiadi, T., et al. (2019). Makassar Strait throughflow seasonal and interannual variability: An overview. *Journal of Geophysical Research: Oceans*, *124*(6), 3724–3736. https://doi.org/10.1029/2018JC014502

Gordon, A. L., Sprintall, J., Van Aken, H. M., Susanto, D., Wijffels, S., Molcard, R., et al. (2010). The Indonesian Throughflow during 2004–2006 as observed by the INSTANT program. *Dynamics of Atmospheres and Oceans*, *50*(2), 115–128. https://doi.org/10.1016/j.dynatmoce.2009.12.002

Gordon, A. L., Susanto, R. D., Ffield, A., Huber, B. A., Pranowo, W., & Wirasantosa, S. (2008). Makassar Strait throughflow, 2004 to 2006. *Geophysical Research Letters*, *35*(24), L24605. https://doi.org/10.1029/2008GL036372

Hatayama, T., Awaji, T., & Akitomo, K. (1996). Tidal currents in the Indonesian Seas and their effect on transport and mixing. *Journal of Geophysical Research*, *101*(C5), 12353–12373. https://doi.org/10.1029/96JC00036

Hirst, A., & Godfrey, J. (1993). The role of Indonesian Throughflow in a global ocean GCM. *Journal of Physical Oceanography*, *23*(6), 1057–1086. https://doi.org/10.1175/1520-0485(1993)023<1057:TROITI>2.0.CO;2

Holloway, P. E. (2001). A regional model of the semidiurnal internal tide on the Australian North West Shelf. *Journal of Geophysical Research*, *106*(C9), 19625–19638. https://doi.org/10.1029/2000JC000675

Huthnance, J. (1973). Tidal current asymmetries over the Norfolk Sandbanks. *Estuarine and Coastal Marine Science*, *1*(1), 89–99. https://doi.org/10.1016/0302-3524(73)90061-3

IOC, IHO, & BODC. (2003). *Centenary edition of the GEBCO digital Atlas, published on CD-ROM on behalf of the intergovernmental oceanographic commission and the inter-national hydrographic organization as part of the general bathymetric chart of the oceans (Technical Report)*. British Oceanographic Data Centre.

Kartadikaria, A. R., Miyazawa, Y., Varlamov, S. M., & Nadaoka, K. (2011). Ocean circulation for the Indonesian Seas driven by tides and atmospheric forcings: Comparison to observational data. *Journal of Geophysical Research*, *116*(C9), C09009. https://doi.org/10.1029/2011JC007196

Kida, S., & Wijffels, S. (2012). The impact of the Indonesian Throughflow and tidal mixing on the summertime sea surface temperature in the Western Indonesian Seas. *Journal of Geophysical Research*, *117*(C9), C09007. https://doi.org/10.1029/2012JC008162

Koch-Larrouy, A., Madec, G., Bouruet-Aubertot, P., Gerkema, T., Bessières, L., & Molcard, R. (2007). On the transformation of Pacific water into Indonesian Throughflow Water by internal tidal mixing. *Geophysical Research Letters*, *34*(4), L04604. https://doi.org/10.1029/2006GL028405

Koch-Larrouy, A., Madec, G., Iudicone, D., Atmadipoera, A., & Molcard, R. (2008). Physical processes contributing to the water mass transformation of the Indonesian Throughflow. *Ocean Dynamics*, *58*(3–4), 275–288. https://doi.org/10.1007/s10236-008-0154-5

Large, W., & Yeager, S. (2009). The global climatology of an interannually varying air–sea flux data set. *Climate Dynamics*, *33*(2–3), 341–364. https://doi.org/10.1007/s00382-008-0441-3

Levier, B., Tréguier, A.-M., Madec, G., & Garnier, V. (2007). Free surface and variable volume in the nemo code. (Tech. Rep.). https://doi.org/10.5281/zenodo.3244182

Liang, L., Xue, H., & Shu, Y. (2019). The Indonesian Throughflow and the circulation in the Banda Sea: A modeling study. *Journal of Geophysical Research: Oceans*, *124*(5), 3089–3106. https://doi.org/10.1029/2018JC014926

Loder, J. W. (1980). Topographic rectification of tidal currents on the sides of Georges Bank. *Journal of Physical Oceanography*, *10*(9), 1399–1416. https://doi.org/10.1175/1520-0485(1980)010<1399:TROTCO>2.0.CO;2

Lyard, F. H., Allain, D. J., Cancet, M., Carrère, L., & Picot, N. (2021). FES2014 global ocean tide atlas: Design and performance. *Ocean Science*, *17*(3), 615–649. https://doi.org/10.5194/os-17-615-2021

Madec, G. (2016). *NEMO reference manual 3.6 STABLE: NEMO ocean engine (Tech. Rep. No. 27)*. Institut Pierre-SimonLaplace (IPSL).

Moat, B. I., Josey, S. A., Sinha, B., Blaker, A. T., Smeed, D. A., McCarthy, G. D., et al. (2016). Major variations in subtropical North Atlantic heat transport at short (5 day) timescales and their causes. *Journal of Geophysical Research: Oceans*, *121*(5), 3237–3249. https://doi.org/10.1002/2016JC011660

Nagai, T., & Hibiya, T. (2015). Internal tides and associated vertical mixing in the Indonesian Archipelago. *Journal of Geophysical Research: Oceans*, *120*(5), 3373–3390. https://doi.org/10.1002/2014JC010592

Nagai, T., Hibiya, T., & Syamsudin, F. (2021). Direct estimates of turbulent mixing in the Indonesian Archipelago and its role in the transformation of the Indonesian Throughflow waters. *Geophysical Research Letters*, *48*(6), e2020GL091731. https://doi.org/10.1029/2020GL091731

National Geophysical Data Center. (2006). *2-minute gridded global relief data (ETOPO2) v2*. NOAA National Centers for Environmental Information). https://doi.org/10.7289/V5J1012Q

Nugroho, D., Koch-Larrouy, A., Gaspar, P., Lyard, F., Reffray, G., & Tranchant, B. (2018). Modelling explicit tides in the Indonesian Seas: An important process for surface sea water properties. *Marine Pollution Bulletin*, *131*, 7–18. https://doi.org/10.1016/j.marpolbul.2017.06.033

Piccioni, G., Dettmering, D., Bosch, W., & Seitz, F. (2019). TICON: TIdal CONstants based on GESLA sea-level records from globally located tide gauges. *Geoscience Data Journal*, *6*(2), 97–104. https://doi.org/10.1002/gdj3.72

Polton, J. A. (2015). Tidally induced mean flow over bathymetric features: A contemporary challenge for high-resolution wide-area models. *Geophysical & Astrophysical Fluid Dynamics*, *109*(3), 207–215. https://doi.org/10.1080/03091929.2014.952726

Pujiana, K., Gordon, A. L., & Sprintall, J. (2013). Intraseasonal Kelvin wave in Makassar Strait. *Journal of Geophysical Research: Oceans*, *118*(4), 2023–2034. https://doi.org/10.1002/jgrc.20069

Ray, R. D., Egbert, G. D., & Erofeeva, S. Y. (2005). A brief overview of tides in the Indonesian Seas. *Oceanography*, *18*(4), 74–79. https://doi.org/10.5670/oceanog.2005.07

Ray, R. D., & Susanto, R. D. (2016). Tidal mixing signatures in the Indonesian Seas from high-resolution sea surface temperature data. *Geophysical Research Letters*, *43*(15), 8115–8123. https://doi.org/10.1002/2016GL069485

Robertson, R. (2010). Tidal currents and mixing at the INSTANT mooring locations. *Dynamics of Atmospheres and Oceans*, *50*(2), 331–373. https://doi.org/10.1016/j.dynatmoce.2010.02.004

Robertson, R. (2011). Interactions between tides and other frequencies in the Indonesian Seas. *Ocean Dynamics*, *61*(1), 69–88. https://doi.org/10.1007/s10236-010-0343-x

Robertson, R., & Ffield, A. (2005). M_2 baroclinic tides in the Indonesian Seas. *Oceanography*, *18*(4), 62–73. https://doi.org/10.5670/oceanog.2005.06

Robertson, R., & Ffield, A. (2008). Baroclinic tides in the Indonesian Seas: Tidal fields and comparisons to observations. *Journal of Geophysical Research*, *113*(C7), C07031. https://doi.org/10.1029/2007JC004677

Santoso, A., England, M. H., Kajtar, J. B., & Cai, W. (2022). Indonesian Throughflow variability and linkage to ENSO and IOD in an ensemble of CMIP5 models. *Journal of Climate*, *35*(10), 3161–3178. https://doi.org/10.1175/JCLI-D-21-0485.1

Sasaki, H., Kida, S., Furue, R., Nonaka, M., & Masumoto, Y. (2018). An increase of the Indonesian Throughflow by internal tidal mixing in a high-resolution quasi-global ocean simulation. *Geophysical Research Letters*, *45*(16), 8416–8424. https://doi.org/10.1029/2018GL078040

Schauer, U., & Losch, M. (2019). "Freshwater" in the ocean is not a useful parameter in climate research. *Journal of Physical Oceanography*, *49*(9), 2309–2321. https://doi.org/10.1175/JPO-D-19-0102.1

Schiller, A. (2004). Effects of explicit tidal forcing in an OGCM on the water-mass structure and circulation in the Indonesian Throughflow region. *Ocean Modelling*, *6*(1), 31–49. https://doi.org/10.1016/S1463-5003(02)00057-4

Sen Gupta, A., McGregor, S., van Sebille, E., Ganachaud, A., Brown, J. N., & Santoso, A. (2016). Future changes to the Indonesian Throughflow and Pacific circulation: The differing role of wind and deep circulation changes. *Geophysical Research Letters*, *43*(4), 1669–1678. https://doi.org/10.1002/2016GL067757

Sprintall, J., Gordon, A. L., Koch-Larrouy, A., Lee, T., Potemra, J. T., Pujiana, K., & Wijffels, S. E. (2014). The Indonesian Seas and their role in the coupled ocean-climate system. *Nature Geoscience*, *7*, 487–492. https://doi.org/10.1038/ngeo2188

Sprintall, J., Gordon, A. L., Murtugudde, R., & Susanto, R. D. (2000). A semiannual Indian Ocean forced Kelvin wave observed in the Indonesian Seas in May 1997. *Journal of Geophysical Research*, *105*(C7), 17217–17230. https://doi.org/10.1029/2000JC900065

Sprintall, J., Gordon, A. L., Wijffels, S. E., Feng, M., Hu, S., Koch-Larrouy, A., et al. (2019). Detecting change in the Indonesian Seas. *Frontiers in Marine Science*, *6*, 257. https://doi.org/10.3389/fmars.2019.00257

Sprintall, J., Potemra, J. T., Hautala, S. L., Bray, N. A., & Pandoe, W. W. (2003). Temperature and salinity variability in the exit passages of the Indonesian Throughflow. *Deep Sea Research Part II: Topical Studies in Oceanography*, *50*(12), 2183–2204. https://doi.org/10.1016/S0967-0645(03)00052-3

Sprintall, J., Wijffels, S., Molcard, R., & Jaya, I. (2010). Direct evidence of the south Java current system in Ombai Strait. *Dynamics of Atmospheres and Oceans*, *50*(2), 140–156. (Modeling and Observing the Indonesian Throughflow). https://doi.org/10.1016/j.dynatmoce.2010.02.006

Sprintall, J., Wijffels, S. E., Molcard, R., & Jaya, I. (2009). Direct estimates of the Indonesian Throughflow entering the Indian Ocean: 2004–2006. *Journal of Geophysical Research*, *114*(C7), C07001. https://doi.org/10.1029/2008JC005257

Susanto, R. D., Ffield, A., Gordon, A. L., & Adi, T. R. (2012). Variability of Indonesian Throughflow within Makassar Strait, 2004–2009. *Journal of Geophysical Research*, *117*(C9), C09013. https://doi.org/10.1029/2012JC008096

Talley, L. D. (2008). Freshwater transport estimates and the global overturning circulation: Shallow, deep and throughflow components. *Progress in Oceanography*, *78*(4), 257–303. https://doi.org/10.1016/j.pocean.2008.05.001

Talley, L. D., & Sprintall, J. (2005). Deep expression of the Indonesian Throughflow: Indonesian intermediate water in the South Equatorial Current. *Journal of Geophysical Research*, *110*(C10), C10009. https://doi.org/10.1029/2004JC002826

Tranchant, B., Reffray, G., Greiner, E., Nugroho, D., Koch-Larrouy, A., & Gaspar, P. (2016). Evaluation of an operational ocean model configuration at 1/12° spatial resolution for the Indonesian Seas (NEMO2.3/INDO12) - Part 1: Ocean physics. *Geoscientific Model Development*, *9*(3), 1037–1064. https://doi.org/10.5194/gmd-9-1037-2016

Umlauf, L., & Burchard, H. (2003). A generic length-scale equation for geophysical turbulence models. *Journal of Marine Research*, *61*(2), 235–265. https://doi.org/10.1357/002224003322005087

van Sebille, E., Sprintall, J., Schwarzkopf, F. U., Sen Gupta, A., Santoso, A., England, M. H., et al. (2014). Pacific to Indian Ocean connectivity: Tasman leakage, Indonesian Throughflow, and the role of ENSO. *Journal of Geophysical Research: Oceans*, *119*(2), 1365–1382. https://doi.org/10.1002/2013JC009525

Vranes, K., Gordon, A. L., & Ffield, A. (2002). The heat transport of the Indonesian Throughflow and implications for the Indian Ocean heat budget. *Deep Sea Research Part II: Topical Studies in Oceanography*, *49*(7), 1391–1410. https://doi.org/10.1016/S0967-0645(01)00150-3

Wei, J., Li, M. T., Malanotte-Rizzoli, P., Gordon, A. L., & Wang, D. X. (2016). Opposite variability of Indonesian Throughflow and South China Sea throughflow in the Sulawesi Sea. *Journal of Physical Oceanography*, *46*(10), 3165–3180. https://doi.org/10.1175/JPO-D-16-0132.1

Wise, A., Harle, J., Bruciaferri, D., O'Dea, E., & Polton, J. (2022). The effect of vertical coordinates on the accuracy of a shelf sea model. *Ocean Modelling*, *170*, 101935. https://doi.org/10.1016/j.ocemod.2021.101935

Wright, D. G., & Loder, J. W. (1985). A depth-dependent study of the topographic rectification of tidal currents. *Geophysical & Astrophysical Fluid Dynamics*, *31*(3–4), 169–220. https://doi.org/10.1080/03091928508219269

Wyrtki, K. (1987). Indonesian through flow and the associated pressure gradient. *Journal of Geophysical Research*, *92*(C12), 12941–12946. https://doi.org/10.1029/JC092iC12p12941